Original research article

Institution of MECHANICAL ENGINEERS
Journal of POWER AND ENERGY

Proc IMechE Part A:
J Power and Energy
2026, Vol. 0(0) 1–28
© IMechE 2026

Article reuse guidelines:
sagepub.com/journals-permissions
DOI: 10.1177/09576509261456450
journals.sagepub.com/home/pia
Sage

# A novel application of TERA framework for gas compressor station performance analysis using thermal modelling assumptions

**Oluwatayo Babatope Ojo, Abdelrahman Hegab, Uyioghosa Igie and Pericles Pilidis**

## Abstract

Gas compressors are critical yet energy-intensive components of pipeline networks. Accurately predicting their performance is a significant design and operational challenge, profoundly affected by the thermal behaviour of the transported gas. This study introduces a novel application of a techno-economic and environmental risk analysis (TERA) framework to determine gas compressor performance under three distinct gas flow temperature assumptions: isothermal, intermediate, and non-isothermal. The analysis, performed in MATLAB R2024a, integrates thermodynamic gas properties, pipeline hydraulics (via the Weymouth equation), and compressor characteristics, explicitly accounting for ambient temperature and altitude variations at each compressor station along the pipeline route. The results demonstrate that the common assumption of isothermal flow yields fixed but potentially inaccurate operating points. In contrast, non-isothermal analysis, which ties gas temperature to fluctuating ambient conditions, reveals significant operational dynamics. Specifically, compressor power demand peaks at 15:00 hours during the hottest season and reaches its lowest point at 06:00 hours during the coldest season, directly correlating with ambient temperature cycles. This fluctuation, which can critically impact design and fuel consumption, is entirely masked in isothermal and intermediate models. Furthermore, the findings show that for every 1% increase in the non-isothermal ambient temperature, the compressor suction pressure decreases by an average 0.1% and the compressor power demand increases by an average 0.3%, corresponding to an average increase of 0.3% in the polytropic head. A ±5% parametric sensitivity analysis confirms that inlet temperature exerts the strongest influence on power demand (±1.5%), followed by mechanical efficiency (±1.0%), pressure ratio (±0.8%), and gas composition (±0.4%). The total estimated annual operational cost for the 18-station pipeline network under isothermal conditions is approximately USD 90.66 million; however, a sensitivity analysis assuming a +10% increase in power demand during daily peaks reveals that operational costs could be underestimated by more than USD 56,000 per year for a single station, demonstrating that the isothermal assumption risks substantial under-estimation of long-term operational expenditures (OPEX). This study provides, for the first time, a comparative analysis of these three scenarios within a unified TERA framework, delivering crucial insights for selecting appropriately sized compressors. The MATLAB model was validated against Aspen HYSYS, showing excellent agreement with a maximum deviation of only 0.348% and a mean absolute deviation of 0.035% across all 18 stations. Therefore, this work offers a robust methodological advance that can assist designers in optimising the design and operation of existing or new long-distance natural gas transmission pipelines, leading to improved economic and operational outcomes.

## Keywords

Non-isothermal, intermediate, isothermal, operating point, ambient temperature, gas thermodynamics, techno-economic, pipeline hydraulics

## Introduction

Natural gas is a crucial fuel used in various industries and sectors of the economy. Its low carbon footprint compared to coal makes it a fuel of choice in countries where renewable energy and other alternative fuels are expensive to obtain. There is a need to transport this gas from surplus locations to areas in short supply. In many cases, these locations are usually thousands of kilometres apart. Therefore, it is imperative to design an efficient transportation system that meets end-user demands under all conditions. Natural gas transportation via pipeline has been identified as an economical and efficient means of gas transportation over long distances to areas with high demand.[1–22] The properties and composition of natural gas significantly influence pipeline operating conditions. These depend on the annual extraction period, the source of production, and the degree of gas treatment.[23] Therefore, any change in the natural gas composition will ultimately

Centre for Aeronautics, Propulsion and Power, Faculty of Engineering and Applied Sciences, Cranfield University, Cranfield, UK

**Corresponding author:**
Oluwatayo Babatope Ojo, Centre for Aeronautics, Propulsion and Power, Faculty of Engineering and Applied Sciences, Cranfield University, Cranfield, MK43 0AL, UK.
Email: o.b.ojo@cranfield.ac.uk

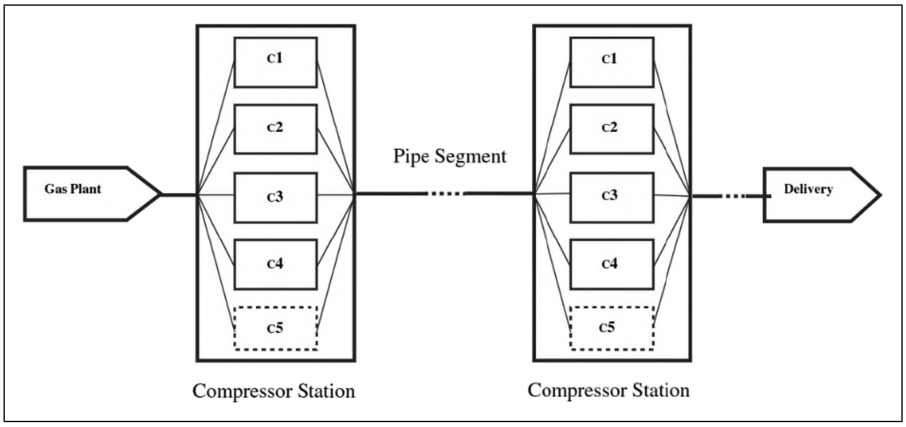



**Figure 1.** Compressor stations and pipe segments schematic.[31]

affect its compressibility factor, gravity, density and other thermophysical properties. These pipelines require that the compressor stations be placed at appropriate distances. This is to ensure the continuous operation of the various components and meet end-users' demands. These stations are thoughtfully positioned at regular intervals along the pipeline and require large areas of land.[24] It is estimated that compressor stations consume about three to five per cent of the total gas transported.[18,25] They accommodate compressors driven by prime movers and are usually installed some kilometres apart along the pipelines.[26–30] Figure 1 illustrates the schematic diagram of the compressor station layout and pipe segments. It features five compressor units arranged in parallel at each station. This includes a gas plant supply node and a delivery terminal at the demand node.

Efficient design of compressor stations and pipeline systems is vital for meeting end-users' demands and minimising transportation costs. After all, an efficient gas transmission network can reduce natural gas consumption at compressor stations by at least 20%.[25] The ambient conditions at the location influence the performance of compressor stations and pipeline systems, the flow rate, and the operation of compressor stations.[32] Hence, understanding the performance of gas compressors in natural gas transmission pipelines is essential for the efficient operation of the system and its components. Therefore, it is crucial to examine various parameters when designing compressor stations and pipelines. This includes ambient conditions, pipe diameter, length, elevation, natural gas properties, and gas compressor performance.[33] Nasir stated that the flow rates of the pipeline depend on factors such as pipe diameter, length, pressure drop from friction, gas suction temperature, suction pressure, and the properties of the gas.[34] Gas compressors are a crucial component of compressor stations and pipeline systems. They supply the pressure energy needed for a constant gas flow through the pipeline. Most long-distance transmission pipelines operate at pressures ranging from 60 to 100 bar. Therefore, it is imperative to compress natural gas to pipeline pressures.[35–37] Natural gas compression is achieved by converting the driver's mechanical energy to kinetic energy in the gas. Multiple gas compressors can be installed in either parallel or series configuration within a compressor station. This is to enhance the pipeline flow rate or increase the outlet pressure.[38] When choosing a compressor for a specific application, it is essential to consider factors such as performance, reliability, availability, and cost. Gas compression is an energy-consuming process since more than 67% of annual operating costs are usually used up by energy utilised for this process.[4] Thus, a minuscule enhancement in efficiency will significantly impact operating

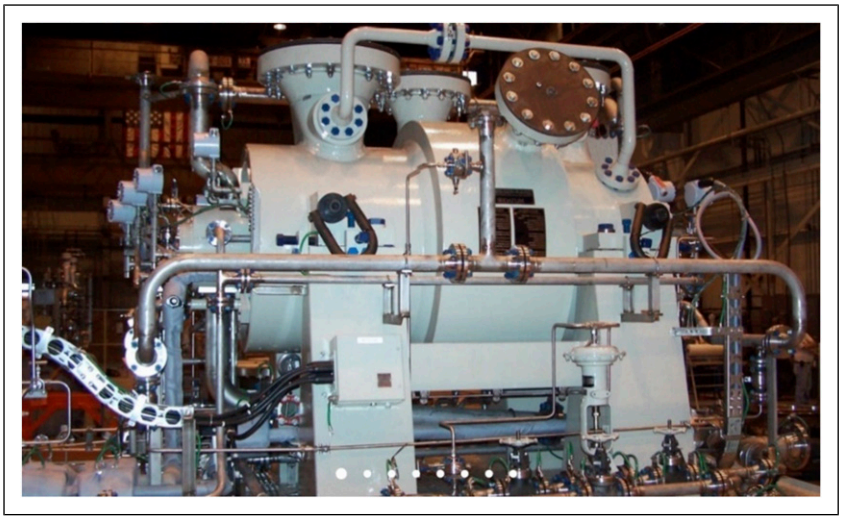


**Figure 2.** Siemens barrel-type STC-SV compressor.[43]

costs. After all, the economic success of a gas compression operation is dependent on gas compressor performance.[27,39–42] The centrifugal compressor is preferred over other compressor types. This is due to its good performance, high availability, low operation and maintenance costs, simple construction, low head, and suitability for high-volume flows. Figure 2 shows Siemens's barrel-type single-shaft pipeline centrifugal compressor.

The operating point of the gas compressor is defined by the compressor map, the driver power, and the head-flow characteristics.[35,44–46] The performance map is created based on compressor selection and from performance analysis. Thereafter, this is utilised to determine its operating conditions by evaluating its head-flow characteristics. Centrifugal compressor performance is a function of inlet volume flow rate, speed, isentropic head, isentropic efficiency,[47,48] and compressor power requirement. The interrelationships among these parameters are shown in performance maps. The original equipment manufacturer can supply the compressor's power requirement, efficiency, and speed after the performance analysis. The compressor's drivers are sized based on the above information and the prevailing ambient conditions. The compressor operating speed is usually varied to control the flow through it. The parameters that affect the centrifugal compressor's operating range are surge flow, choke, driver power, and maximum and minimum speeds. The performance curve of a turbo-compressor at constant wheel revolutions is restricted at both the low and high flow rates by the surge and stonewall points. Compressor surge is characterised by periodic gas flow in the compressor and the connected piping system. During part of the cycle, there is a backward flow. Surge flow occurs when the compressor operates at a lower flow rate, resulting in flow reversal and fluctuating bearing loads.[42,49–56] It is an unstable condition, causing pressure oscillation that results in compressor damage, including the connected piping system.[57–61] Control systems are designed to detect and prevent surges. This protects the compressor from damage. They must keep the compressor's operating point within its safe operating range. This is done to avoid instabilities that cause breakdowns and engine downtime.[39] The Stonewall line is a phenomenon that occurs when the gas compressor speed reaches the speed of sound. This produces shockwaves that cause vibration in the parts.[62,63] When the machine is operating at the stonewall point, the flow in the blade systems (wheel and bladed diffuser) is choked by shock waves. The flow can be unsteady. The acceptable operating range will be the enclosed area on the performance map. This takes into account safety, stability, and the anti-surge protection line. Figure 3 shows a typical centrifugal compressor map.

Meira et al.[62] have proposed a new approach to performance modelling of compressor maps for natural gas pipelines. This work builds on the National Aeronautics and Space Administration's loss theory to estimate energy losses. This includes accurately deriving the compressor characteristic curves, as well as the surge and choke lines. The results highlight the advantages of this modelling approach over conventional models. Thus, demonstrating its crucial role in reducing the operational costs of compressor stations. The reliability and validity of off-design simulations depend on performance maps. This should be assessed using available data, provided the engine's design-point information is known.[65–70] Therefore, the efficient operation of the compressor station and pipeline systems will depend significantly on the gas compressor performance maps, which are influenced by ambient conditions at the compressor station along the pipeline route. Several authors have investigated the performance of pipelines and gas compressors, accounting for ambient conditions. Albusaidi and Pilidis present an iterative method to determine the equivalent performance of centrifugal compressors under various operating conditions.[71,72] This method accounts for changes in gas properties and stage efficiency, making it appropriate for hydrocarbon fuels. It was used to evaluate the performance of two multistage centrifugal compressors and compare their characteristics with measured data. The results demonstrated a strong agreement with the original values. Osiadacz and Chaczykowski compared isothermal and non-isothermal models of gas flow in pipelines.[73] The analysis revealed significant differences in pressure profiles along the gas pipeline.[74,75] Sanaye and Mahmoudimehr have conducted both isothermal and non-isothermal modelling of a gas pipeline, accounting for ground

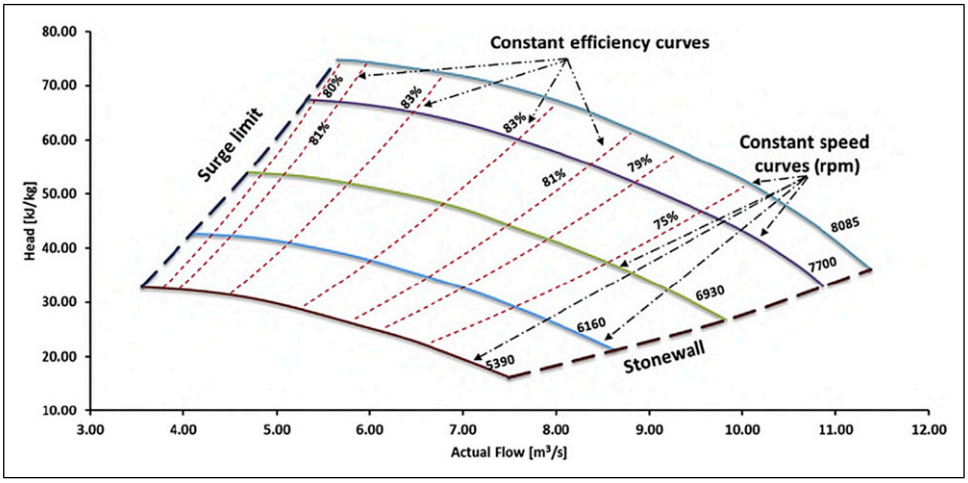



**Figure 3.** Centrifugal compressor map.[64]

temperature effects.[75] They derived a new form of conservation equations for compressible flow.[76] The results indicate a maximum difference of approximately 33.7% in the compressor head and 16.6% in rotational speed. This is based on established natural gas properties at various points along the pipeline. Lopez-Benito et al.[77] developed a numerical method to integrate a mathematical model that describes the flow in a natural gas pipeline under non-isothermal steady-state conditions. They transformed the model equations into a system of three explicit expressions for the spatial derivatives of the gas velocity, temperature, and pressure. This proposed method enables the prediction of gas pressure, temperature, and velocity at any point along the pipeline. However, these studies did not estimate the power requirements for gas compressors using the TERA approach. More so, these studies did not simultaneously account for isothermal, intermediate, and non-isothermal gas flow in pipelines. Additionally, they did not evaluate the performance maps of gas compressors under both design and off-design conditions, accounting for variations in gas flow temperature to assess the performance of both the gas compressor and the pipeline system.

Recent developments in the field have increasingly focused on thermodynamic optimisation and real-time monitoring of compressor station performance. Yang and Xuejiang.[78] applied Modular Dynamic System Greitzer (MDSG) compressor digital twin modelling and Short-Time Fourier Transform, Convolutional neural network (STFT-CNN) algorithm for recognising the surge case of series compressor systems. The average errors in the inlet and outlet pressures of a real suction compressor system are 1.88% and 0.67%, respectively. The accuracies of the training and test sets of the STFT-CNN method for compressor anomaly monitoring are 99.58% and 98.75%, respectively. Their results demonstrated that a digital twin model integrated with a condition-monitoring network can enable real-time simulation and monitoring of the compressor system. Similarly, Kai et al.[79] proposed a digital twin-driven intelligent control of a natural gas flowmeter calibration station to improve the efficiency of flowmeter calibration. The results show that the proposed method can accurately obtain the hydraulic state and control strategy and considerably enhance the calibration efficiency. Recent studies have proposed various machine learning-enhanced thermodynamic models for centrifugal compressor performance prediction, including Whale Optimisation Algorithm back-propagation neural network (WOA-BPNN),[80] similarity- and scaling-laws-informed neural networks (SINN).[81] The prediction accuracy of the proposed models is found to be better than conventional methods. Furthermore, Ojo et al.[14] conducted a techno-economic optimisation of the compressor station and pipeline segments for the proposed Trans-Saharan Gas Pipeline (TSGP) project under variable ambient conditions. The 4180 km pipeline would carry natural gas from Nigeria to Algeria's export terminal on the Mediterranean Sea and eventually supply Europe. The optimisation problems were formulated to minimise lifecycle cost, with the location of the compressor stations as the decision variable. The results showed 12 compressor station locations along the pipeline route in one of the optimised cases. The optimised lifecycle cost is reduced by 12.95% compared to the baseline case. The optimised compressor station locations were at 1, 38, 76, 113, 150, 186, 222, 260, 296, 332, 368, and 408 segments of the pipeline. While these studies have advanced the state of the art, none have simultaneously evaluated all three thermal flow regimes (isothermal, intermediate, and non-isothermal) within a unified TERA framework that links pipeline hydraulics, compressor performance maps, and economic analysis, as is done in the present study.

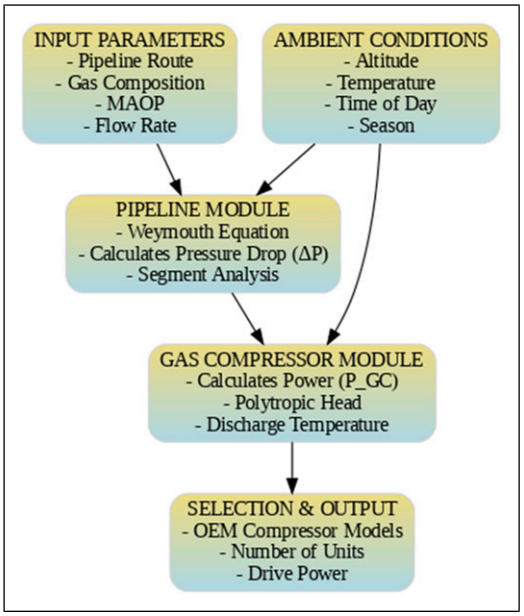



**Figure 4.** Flowchart of the Techno-Economic and Environmental Risk Analysis (TERA) framework used in the present study. The integrated model processes input parameters through sequential pipeline and compressor modules, conditioned by the ambient data, to produce technical and economic outputs for compressor selection.

Therefore, the objective of this study is to determine the power requirements of compressor stations under different gas-flow temperature conditions. This analysis is based on three flow assumptions: isothermal, intermediate, and non-isothermal. The study utilises the techno-economic and environmental risk analysis (TERA) framework to guide the evaluation of natural gas flow in pipelines. This study presents the following information for the first time:

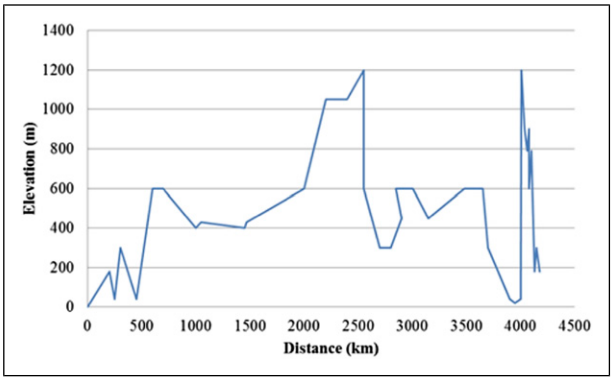



**Figure 5.** Pipeline elevation-distance profile.[82]

What gas compressor sizes are needed for different flow conditions at each compressor station location, considering isothermal, intermediate, and non-isothermal gas flow temperature assumptions based on the TERA approach?
What are the effects of gas compressor powers at isothermal, intermediate, and non-isothermal gas flow temperature conditions?
What are the impacts of gas compressor operating points at varying flow conditions?
How do we select appropriate gas compressors based on the analysis?

The remainder of this paper is organised as follows. The Methodology presents and describes the modules that comprise the TERA framework. Gas compressor powers were evaluated under varying flow conditions, and performance maps were generated using scaling analysis. The essential outcome of the study is presented in the results and discussion section. Subsequently, the study's conclusion and limitations are highlighted, and directions for future research are suggested.

## Methodology

This study employs an integrated analytical approach to assess the power requirements of compressor stations under varying thermal flow regimes. The core of the methodology is the Techno-economic and Environmental Risk Analysis (TERA) framework, implemented in MATLAB environment, which synthesises pipeline hydraulics, gas thermodynamics, and compressor performance. The overarching process, visualised in the flowchart in Figure 4, is summarised as follows:

**Input & Initiation:** The process begins with the input of fixed parameters obtained from the preliminary report on the proposed Trans-Saharan Gas Pipeline.[27] These include pipeline geometry (diameter, length, elevation profile), natural gas composition, required flow rate, and the Maximum Allowable Operating Pressure (MAOP).
**Pipeline Hydraulic Module:** The input parameters feed into the pipeline module, which calculates the pressure drop along each pipeline segment between compressor stations. Using the Weymouth equation, it accounts for pipe geometry, gas properties, elevation profile (Figure 5), and crucially, the gas flowing temperature, which is defined by one of three scenarios.
**Gas Compressor Module:** The resulting outlet pressure from the pipeline module defines the suction pressure for a compressor station. This module then calculates the required compressor power, polytropic head, and discharge temperature based on this suction pressure and the gas suction temperature (again, defined by the scenario).
**Ambient Conditioning:** Crucially, both the pipeline and gas compressor modules are continuously influenced by the local ambient conditions (altitude, temperature, time of day, season) at each station. This is the key driver for simulating non-isothermal flow. These ambient conditions are environmental variable that influences compressor performance and techno-economics. The ambient conditions at the stations along the pipeline route correspond to the environmental-risk component of the TERA framework since the pipeline is assumed to be clean. Therefore, the variation in local ambient conditions at each station, as demonstrated by the considered scenarios, serves as a key measure of environmental risk that influences the techno-economic outputs.
**Output & Selection:** The final outputs are the compressor power requirements and performance maps under each scenario. These results directly guide the techno-economic selection of appropriate compressor models from original equipment manufacturer (OEM) databases, ensuring they can meet the demands of all observed operating conditions.

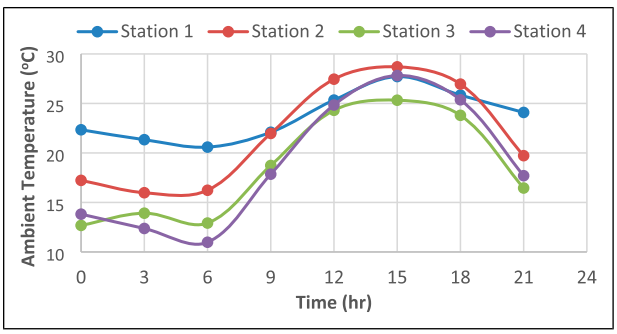



**Figure 6.** Ambient temperatures recorded at various stations during the winter season.

The subsequent sections detail the assumptions, environmental data, and specific mathematical models that underlie this framework.

### *Environmental conditions*

The altitude and ambient conditions at the compressor station along the pipeline route will significantly affect the gas compressor's performance. The altitude at which the compressor station and pipeline operate will affect the gas compressor's performance because altitude significantly affects ambient temperature. Therefore, ambient temperature and altitude at the location should be considered when assessing the gas compressor performance. The average daily ambient temperature for the location where the compressor station would be installed was obtained from the Trans-Saharan Gas Pipeline report.[27] The elevation-distance profile was retrieved from Ref. 82. Figure 5 shows the pipeline elevation-distance profile utilised in this study.[82] Figure 6 illustrates the cumulative three-hourly variation in ambient temperature during one season of the year, relating to the time of day at the compressor stations along the pipeline route. This study uses the average temperature for each season, assuming 4 months per season.

The ambient conditions form the basis for analysing the pipeline and gas compressor models in this study.

These operating conditions have a significant impact on the techno-economics of the proposed Trans-Saharan Gas Pipeline project.

## Pipeline and gas compressor model assumptions

The following shows the assumptions utilised in the analysis of the pipeline and gas compressor models:

1. Constant pipe diameter for the whole pipeline length.
2. Constant natural gas composition.
3. The gas flow temperature is assumed to be equal to the location's ambient temperature at the compressor station's suction or discharge point.[83]
4. Baseline case comprises 18 compressor stations in a predetermined location.
5. The pipeline is clean.
6. The operation of the gas compressors is based on the variation in the station location ambient temperatures at varying gas flow temperature conditions.
7. The selected gas compressors are expected to operate over the project lifecycle.

The limitations introduced by assuming constant pipe diameter, constant gas composition, clean pipeline conditions, and steady-state thermal behaviour are that, with a constant pipe diameter, variations in flow conditions are mostly influenced by temperature and pressure changes along the pipeline. A constant gas composition is valid for steady-state thermal analysis. A steady state thermal treatment ignores the transient and therefore limits full compressor analysis, while clean pipeline conditions provide no information about degradation over the project lifecycle.

## Gas properties calculation and pipeline pressure drop

The natural gas molecular weight is estimated using a weighted average method from the known component's gas properties as follows:

$$MW = \sum_{j=1}^{N} y_j MW_j \tag{1}$$

Where, $MW_j$ represents the molecular weight of the $j$ th component, and $y$ denotes its volume fraction in a gas mixture.

The natural gas gravity $G$, an estimate of the degree of its weight relative to air at a specified reference temperature is calculated as follows:

$$G = \frac{MW}{MW_{air}} \tag{2}$$

The ideal gas equation of state is modified to the real gas equation of state by considering compressibility effects, as natural gas pipelines often operate at higher pressures. The real gas equation of state can be expressed as:

$$Pv = ZRT_f \tag{3}$$

Where:
$P$ = Total pressure, kPa
$v$ = S
pecific molar volume, $m^3$/kmol
$Z$ = Compressibility factor
$R$ = Universal gas constant, kJ $kg^{-1}$ $K^{-1}$
$T_f$ = Gas flow temperature, K

The compressibility factor $Z$ is an important measure that indicates how closely real gases behave like ideal gases. This factor depends on various parameters, including gas gravity, pressure, temperature, and the composition of natural gas. It can be calculated using the method provided by the California Natural Gas Association as follows:[83]

$$Z = \frac{1}{\left[1 + \left(\frac{344400 * P_{avg} * (10)^{1.785G}}{(T_f)^{3.825}}\right)\right]} \tag{4}$$

where, $P_{avg}$ represents the average pressure of natural gas in the pipe segment. As the compressibility factor changes with pressure, it will vary along the length of the pipeline. Thus, the compressibility factor is estimated using the average pressure of the gas along the pipeline. The average gas pressure for a pipe segment, with a discharge pressure of $P_1$, and a suction pressure of $P_2$, is defined by:[83]

$$P_{avg} = \frac{2}{3}\left(P_1 + P_2 - \frac{P_1 * P_2}{P_1 + P_2}\right) \tag{5}$$

The average pressure is used to calculate the compressibility factor of natural gas at the flowing temperature. The equation for the compressibility factor is applicable when the average gas pressure exceeds 690 kPa; Otherwise, a value of one is assumed.

The Weymouth equation is used for pipelines that transport natural gas over long distances, with high gas throughput and pressure, and with large diameters.[4,27,84] It calculates the natural gas flow rate at a given pressure without using a friction factor. Instead, it accounts for the pipe's internal conditions using a pipeline efficiency factor. Thus, ensuring accurate evaluation of

**Table 1.** Pipeline data for compressor station 2

| S/N | Parameters | Values (Units) |
|---|---|---|
| 1. | Natural gas flow | 30 (bcm/year) |
| 2. | Pipe nominal diameter | 1422.4 (mm) |
| 3. | Pipe outer diameter | 1422.4 (mm) |
| 4. | Pipe inner diameter | 1381.2 (mm) |
| 5. | Wall thickness | 20.62 (mm) |
| 6. | Gas gravity | 0.6048 (mm) |
| 7. | Compressibility factor | 0.8738 |
| 8. | Gas temperature | 308.56 (K) |
| 9. | Base temperature | 288.15 (K) |
| 10. | Base pressure | 101 (bar) |
| 11. | MAOP | 95 (barg) |
| 12. | Elevation | 200 (m) |
| 13. | Equivalent Length | 243.7 (km) |
| 14. | Efficiency | 0.918 |
| 15 | Pipe inlet pressure | 95 (bar) |
| 16. | Pipe outlet pressure | 63 (bar) |

pressure drop over other methods, such as the classical Darcy-Weisbach method.

For a given pipe inlet pressure $P_1$, natural gas flow rate Q, gas gravity $G$, gas compressibility $Z$, pipe length $L$, and pipe constant diameter $D$, the pipe outlet pressure $P_2$, from each pipeline segment, is calculated using the Weymouth gas flow equation in S.I. units as follows:

$$P_2 = \left[\left({P_1}^2 - \frac{7.136\times10^4 Q^2 {P_b}^2 G T_f L_e Z}{{T_b}^2 E^2 D^{5.334}}\right) exp(-s)\right]^{0.5} \quad (6)$$

The equivalent length $L_e$, accounts for elevation differences between the ends of each pipe segment and is given by:

$$L_e = \frac{L(e^s - 1)}{s} \quad (7)$$

Where:
$L$ = Pipe length, km
$s$ = Elevation adjustment parameter

The elevation adjustment parameter $s$, depends on the compressibility factor, gravity, and flow temperature of the gas, including the pipe segment's elevation difference and is given as:

$$s = 6.84\times10^{-2} G\left(\frac{H_2 - H_1}{T_f Z}\right) \quad (8)$$

Where:
$H_1$ = Upstream elevation, m
$H_2$ = Downstream elevation, m
$Z$ = Compressibility factor
$T_f$ = Gas flow temperature, K$G$ = Gas gravity

Hence, the pressure drop along the natural gas transmission pipeline segment is the algebraic difference between the estimated outlet pressure of the pipe and the known inlet pressure defined by:

$$\Delta P = P_1 - P_2 \quad (9)$$

Table 1 presents the pipeline data for Compressor Station 2.

## Gas compressor model

The compression ratio of the gas compressor at each station is evaluated as follows:

$$Compression\ ratio = \frac{P_1}{P_2} \quad (10)$$

Where:
$P_1$ = Gas compressor discharge pressure, kPa
$P_2$ = Gas compressor suction pressure, kPa

The discharge temperature of the gas compressor for a polytropic process depends on the gas compressor inlet temperature, compression ratio, polytropic exponent and the compressibility factors and is defined by:

$$T_1 = T_2\left(\frac{Z_2}{Z_1}\right)\left(\frac{P_1}{P_2}\right)^{\frac{(n-1)}{n}} \quad (11)$$

Where:
$T_1$ = Gas compressor discharge temperature, K
$T_2$ = Gas compressor suction temperature, K
$Z_2$ = Compressibility factor at suction condition
$Z_1$ = Compressibility factor at discharge condition
$P_1$ = Gas compressor discharge pressure, kPa
$P_2$ = Gas compressor suction pressure, kPa
$n$ = Polytropic exponent

The gas compressor discharge temperature can strain the compressor components and reduce its reliability. Therefore, it is crucial to regulate this temperature by adequate cooling or maintaining it within an acceptable range. Liu et al.[85] have investigated a three-dimensional simplified model of an air cooler for a natural gas compressor station. This model is used to simulate and study the cooling effect of a finned-tube dry air cooler

**Table 2.** Distance, elevation, and ambient temperatures recorded at various stations.

| | | | Average ambient temperature (°C) | | |
|---|---|---|---|---|---|
| Station no | Distance (km) | Elevation (m) | Scenario 1 | Scenarios 2 (Peak) | Scenario 3 |
| 1 | 240 | 100 | 22 | 31.7 | 24.5 |
| 2 | 240 | 200 | 22 | 35.4 | 23.6 |
| 3 | 240 | 600 | 22 | 31.9 | 21.2 |
| 4 | 240 | 402 | 22 | 34.7 | 23.0 |
| 5 | 240 | 400 | 22 | 34.7 | 23.0 |
| 6 | 240 | 400 | 22 | 34.7 | 23.0 |
| 7 | 230 | 480 | 22 | 35.6 | 24.2 |
| 8 | 250 | 600 | 22 | 32.0 | 21.2 |
| 9 | 230 | 800 | 22 | 31.9 | 17.0 |
| 10 | 230 | 1050 | 22 | 25.8 | 10.1 |
| 11 | 230 | 400 | 22 | 34.6 | 22.9 |
| 12 | 230 | 400 | 22 | 34.7 | 23.0 |
| 13 | 230 | 560 | 22 | 39.6 | 23.2 |
| 14 | 230 | 480 | 22 | 35.6 | 24.2 |
| 15 | 230 | 600 | 22 | 31.9 | 21.1 |
| 16 | 230 | 900 | 22 | 31.7 | 17.1 |
| 17 | 230 | 700 | 22 | 36.2 | 19.0 |
| 18 | 190 | 240 | 22 | 40.6 | 26.6 |

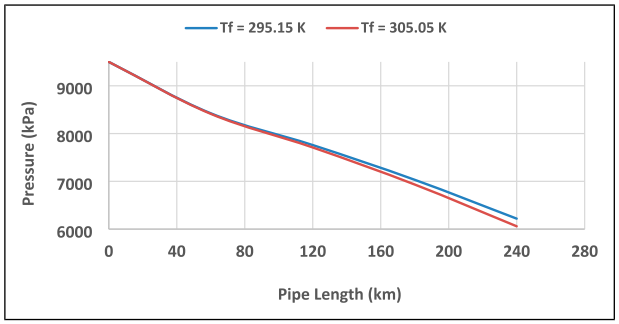



**Figure 7.** Pressure drops along the pipeline for compressor station 3

on high-temperature, high-pressure natural gas at the compressor outlet. The polytropic head generated by the gas compressor represents the amount of energy delivered to the natural gas per unit mass.[86] It depends on the inlet temperature, molecular weight, compression ratio, compressibility factor, and polytropic exponent. It is defined by:

$$H_p = Z_{avg} R T_f \frac{n}{n-1}\left[\left(\frac{P_2}{P_1}\right)^{\frac{-(n-1)}{n}} - 1\right] \quad (12)$$

Where:
$H_p$ = Polytropic head, kJ/kg
$Z_{avg}$ = Average gas compressibility factor
$R$ = Gas constant, kJ $kg^{-1}$ $K^{-1}$
$T_f$ = Gas flow temperature, K

The gas compressor power requirement can be written as:

$$P_{GC} = \frac{mH_p}{3600\eta_p} \quad (13)$$

Where:
$P_{GC}$ = Gas compressor power, kW
$H_p$ = Polytropic head, kJ/kg
$\eta_p$ = Polytropic efficiency$m$ = Mass flow rate, kg/h

The polytropic efficiency $\eta_p$, is independent of the thermodynamic properties of the gas but depends on the isentropic exponent $k$, and the polytropic exponent $n$. It is defined as follows:

$$\eta_p = \frac{\left({}^{n}/_{n-1}\right)}{\left({}^{k}/_{k-1}\right)} \quad (14)$$

The gas compressor's actual volume flow rate at suction conditions $Q_{act}$, is given by:

$$Q_{act} = QZ_2\left(\frac{P_b}{P_2}\right)\left(\frac{T_f}{T_b}\right) \quad (15)$$

Where:
$Q_{act}$ = Actual volume flow rate, m3/hour
$Q$ = Gas volumetric flow rate, m3/day
$Z_2$ = Compressibility factor at suction
$P_b$ = Base pressure, kPa
$P_2$ = Gas compressor suction pressure, kPa
$T_f$ = Gas flow temperature, K
$T_b$ = Base temperature, K

The gas compressor's actual mass flow rate $m_{act}$, at suction conditions is given by:

$$m_{act} = Q_{act}\rho_s \quad (16)$$

Where, $\rho_s$ is the suction density given by:

$$\rho_s = \frac{P_2}{Z_2 R T_f} \quad (17)$$

Changes in gas flow temperature will affect the actual volumetric flow rate. This is because the gas compressor's suction conditions depend on pressure and temperature.

## *Gas compressor power evaluation at varying flow conditions*

The effect of gas compressor powers at varying gas flow temperature conditions was evaluated in this study. This is based on three scenarios that assume the gas flow temperature matches the location's ambient temperature at the gas compressor station's suction or discharge point.[83] The scenarios are described as follows:

1. Scenario 1 depicts the isothermal gas flow temperature condition. This condition assumes a constant gas-flow temperature of 22°C at all times of the day and in all seasons of the year.

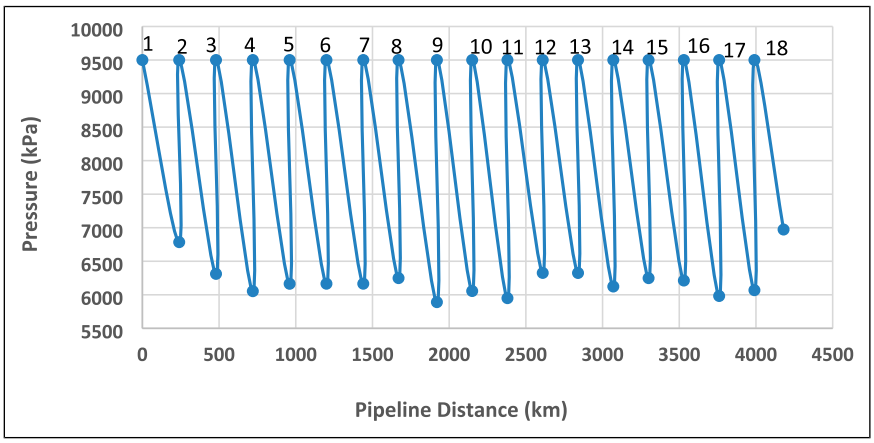



**Figure 8.** Pipeline pressure drops at various compressor station locations.

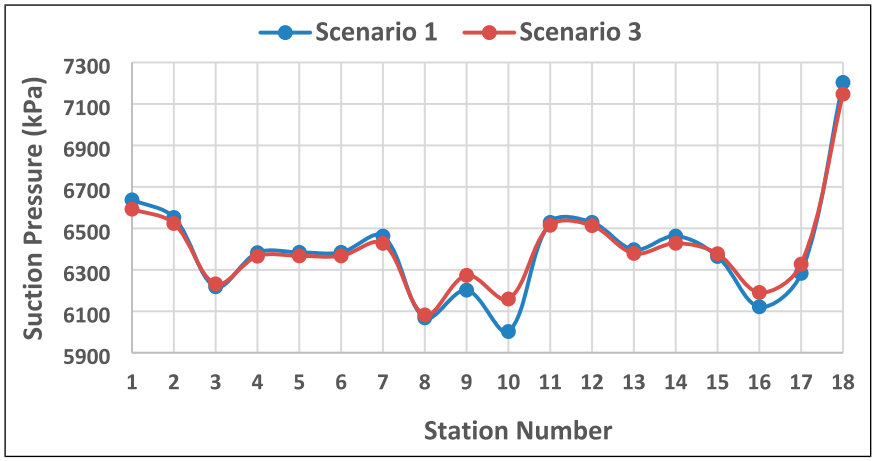



**Figure 9.** Gas compressor suction pressure for Scenarios 1 and 3

2. Scenario 2 depicts the non-isothermal gas flow temperature condition. This condition assumes that the prevailing location time-based ambient temperature is equivalent to the gas-flow temperature. This depends on the ambient temperature variation across the three seasons: winter, dry, and hot. A change in the ambient temperature at the gas compressor station location leads to an equivalent change in the gas flow temperature at the reference time.
3. Scenario 3 depicts the intermediate gas flow temperature condition. This scenario assumes a constant average value for the isothermal and non-isothermal gas flow conditions described above. This value remains constant, as in scenario 1, for all times of the day and throughout all seasons of the year. However, they depend on the prevailing time-based non-isothermal ambient temperature at each gas compressor station.

Table 2 lists every compressor station, along with distance, elevation, and average ambient temperature for each scenario.

The pipeline inlet pressure is 9500 kPa. The operational constraint is the pipeline's maximum allowable operating pressure of 9500 kPa. Furthermore, all gas compressors installed at each compressor station along the pipeline route are expected to have a pressure ratio between 1.40 and 1.66, as suggested by the Trans-Saharan Gas pipeline report.[27] The three scenarios described the different operating conditions of the gas compressor. The basis for the isothermal modelling assumption (Scenario 1) is that transmission pipelines at gas compressor stations may be insulated, adiabatic, and installed at locations where heat exchange between the gas and its surroundings is sufficient to maintain a constant temperature. This is most applicable to buried pipelines, which are installed below ground level, where the ground temperature exerts a dominant thermal influence, causing the gas temperature to approach it with little or no change. An insulated pipeline is integrated with insulating material to regulate gas temperature and prevent heat losses. Therefore, the assumption of an isothermal model is justified as one of the scenarios considered in this study. However, in real life, ambient temperature varies with the time of day and the season. Pipelines with above-ground segments are usually installed partially or entirely above the ground surface, exposing them to ambient conditions. For the long-distance Trans-Saharan Gas Pipeline route considered in this study, with above-ground sections exposed to diurnal ambient variation, this isothermal modelling assumption is expected to introduce a systematic deviation in compressor power of approximately 2–5% relative to the non-isothermal case. It is important to note that insulation can be applied to either

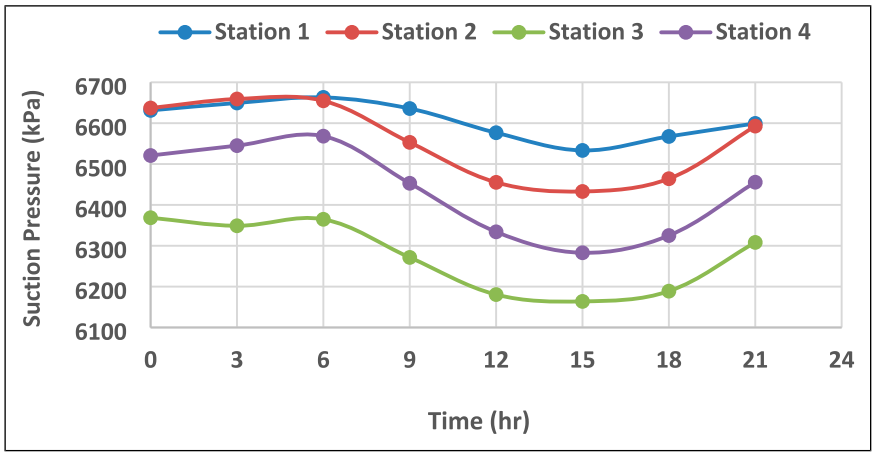



**Figure 10.** Gas compressor suction pressures for Scenario 2

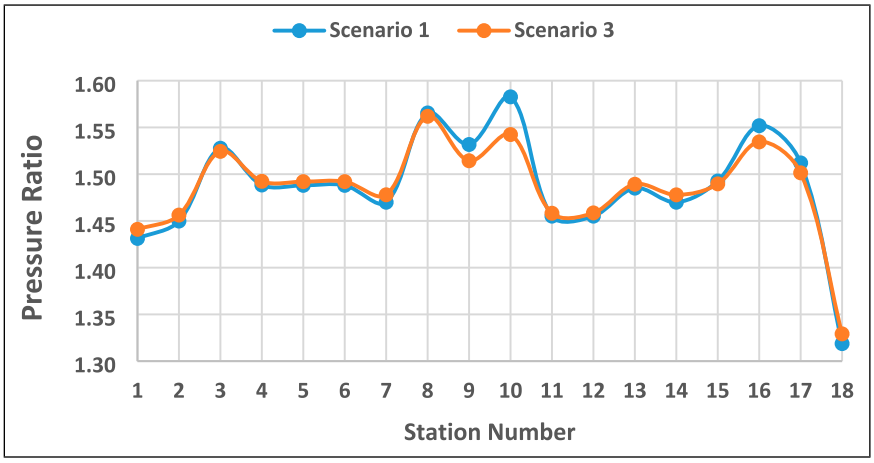



**Figure 11.** Gas compressor pressure ratio for Scenarios 1 and 3

buried or above-ground pipelines. The intermediate thermal model (Scenario 3) assumes a constant average value between the isothermal and non-isothermal models. The intermediate assumption uses a time-averaged temperature that captures mean seasonal conditions; it reduces the error relative to the isothermal case but still underestimates peak power demand by approximately 1–3%. The non-isothermal assumption (Scenario 2), which directly equates gas flow temperature to the local time-varying ambient temperature, represents the most physically realistic scenario for above-ground and surface-laid segments and introduces no systematic bias relative to real-world ambient-driven operation; its residual uncertainty arises primarily from the accuracy of the input ambient temperature data (±0.5–1°C typical for meteorological records), leading to an estimated power uncertainty of less than ±0.5%. All three assumptions are valid for steady-state, fully developed flow in single-phase dry natural gas pipelines operating within the pressure range of 60–100 bar considered in this study. These conditions are expected in the oil and gas industry, which deals with long-distance transmission pipelines. Consequently, they show the full range of temperatures experienced at the gas compressor stations and along the pipeline routes.

By combining equations (12) and (13), the gas compressor powers based on the three scenarios are defined as follows:

$$P_{GC1} = \frac{mZ_{avg}RT_{f1}\frac{n}{n-1}\left[\left(\frac{P_{21}}{P_1}\right)^{\frac{-(n-1)}{n}} - 1\right]}{3600\eta_p} \tag{18}$$

$$P_{21} = \left[\left(P_1^{\,2} - \frac{7.136\times10^4 Q^2 P_b^{\,2} G T_{f1} L_e Z}{T_b^{\,2} E^2 D^{5.334}}\right) exp(-s)\right]^{0.5} \tag{19}$$

Where:

$P_{GC1}$ = Gas compressor power at isothermal flow condition, kW

$P_{21}$ = Gas compressor suction pressure at isothermal flow condition, kPa

$T_{f1}$ = Gas flow temperature at isothermal flow condition, K

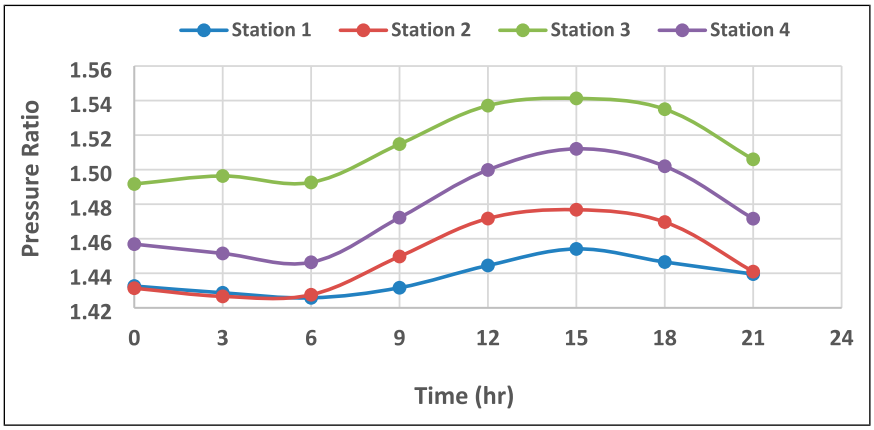



**Figure 12.** Gas compressor pressure ratio for Scenario 2

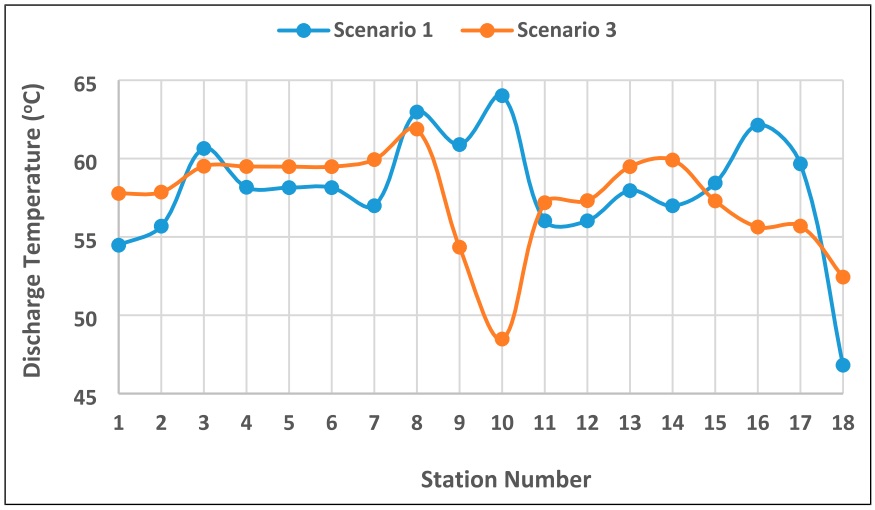



**Figure 13.** Gas compressor discharge temperature for Scenarios 1 and 3

$$P_{GC2} = \frac{mZ_{avg}RT_{f2}\frac{n}{n-1}\left[\left(\frac{P_{22}}{P_1}\right)^{\frac{-(n-1)}{n}} - 1\right]}{3600\eta_p} \quad (20)$$

$$P_{22} = \left[\left(P_1^{\,2} - \frac{7.136\times10^4 Q^2 P_b^{\,2} G T_{f2} L_e Z}{T_b^{\,2} E^2 D^{5.334}}\right) exp(-s)\right]^{0.5} \quad (21)$$

Where:
$P_{GC2}$ = Gas compressor power at non-isothermal flow condition, kW
$P_{22}$ = Gas compressor suction pressure at non-isothermal flow condition, kPa
$T_{f2}$ = Gas flow temperature at non-isothermal flow condition, K

$$P_{GC3} = \frac{mZ_{avg}RT_{f3}\frac{n}{n-1}\left[\left(\frac{P_{23}}{P_1}\right)^{\frac{-(n-1)}{n}} - 1\right]}{3600\eta_p} \quad (22)$$

$$P_{23} = \left[\left(P_1^{\,2} - \frac{7.136\times10^4 Q^2 P_b^{\,2} G T_{f3} L_e Z}{T_b^{\,2} E^2 D^{5.334}}\right) exp(-s)\right]^{0.5} \quad (23)$$

Where:
$P_{GC3}$ = Gas compressor power at intermediate flow condition, kW
$P_{23}$ = Gas compressor suction pressure at intermediate flow condition, kPa
$T_{f3}$ = Gas flow temperature at intermediate flow condition, K

## Gas compressor performance map

The performance maps of gas compressors illustrate how power, polytropic head, pressure ratio, efficiency, and discharge temperature vary with actual volume flow rates at different speeds. The gas compressor performance maps were generated from scaling analyses of the original equipment manufacturer's maps. The steps utilised in obtaining the corrected volume flow rate for the new maps are outlined below:

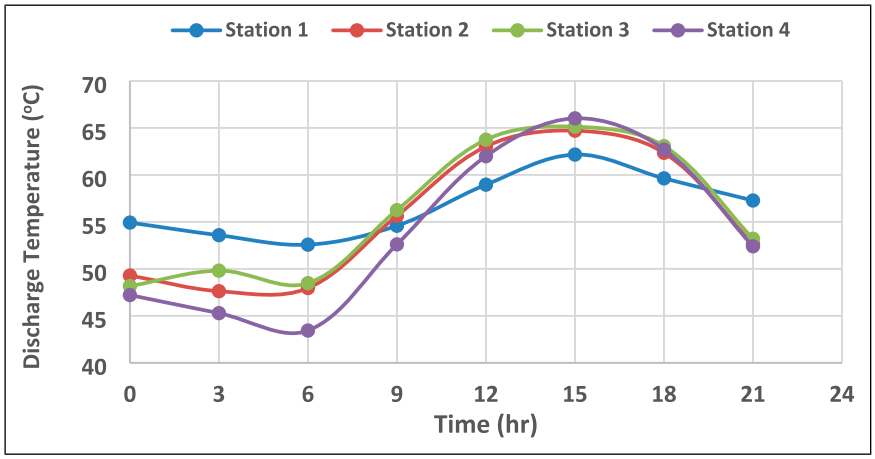



**Figure 14.** Gas compressor discharge temperature for Scenario 2

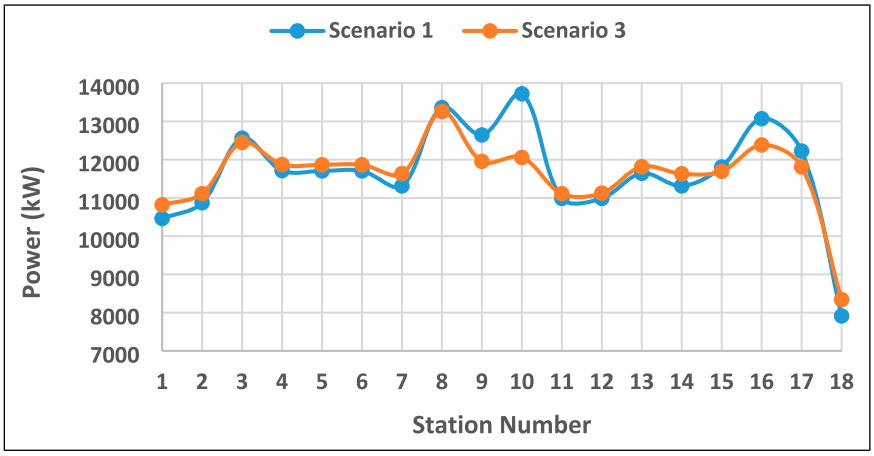



**Figure 15.** Gas compressor power requirement for Scenarios 1 and 3

i. Obtain the actual volume flow at the design point from the original equipment manufacturer's map
ii. Correct this flow
iii. Obtain the actual volume flow at the design point for the new map
iv. Correct this flow
v. Obtain the scaling factor for the corrected volume flows
vi. Obtain the actual volume flow at off-design conditions from the original equipment manufacturer's map
vii. Correct these flows
viii. Obtain the corrected volume flow at off-design conditions for the new map using the scaling factor obtained in item v
ix. Obtain the actual volume flow for these corrected flows for the new map

The corrected mass flow rate $\dot{m}_c$, incorporating humidity effects for a constant diameter machine, such as the gas compressor, is given as:[87]

$$\dot{m}_c = \dot{m_{act}} \frac{\rho_{ref} a_{ref}}{\rho_{act} a_{act}} \tag{24}$$

Where $\rho_{ref}$ is the reference gas density given by:

$$\rho_{ref} = \frac{P_{ref}}{Z_{ref} R_{ref} T_{ref}} \tag{25}$$

$\rho_{act}$ is the actual gas density given by:

$$\rho_{act} = \frac{P_{act}}{Z_{act} R_{act} T_{act}} \tag{26}$$

$a_{ref}$ is the sound speed at the reference condition defined by:

$$a_{ref} = \sqrt{k_{ref} Z_{ref} R_{ref} T_{ref}} \tag{27}$$

$a_{act}$ is the actual sound speed defined by:

$$a_{act} = \sqrt{k_{act} Z_{act} R_{act} T_{act}} \tag{28}$$

Where:
$k_{ref}$ = Polytropic exponent at reference condition
$Z_{ref}$ = Compressibility factor at reference condition
$R_{ref}$ = Gas constant at reference condition, kJ $kg^{-1}$ $K^{-1}$
$T_{ref}$ = Reference temperature, K
$k_{act}$ = Actual polytropic exponent
$Z_{act}$ = Actual compressibility factor$R_{act}$ = Actual gas constant, kJ $kg^{-1}$ $K^{-1}$
$T_{act}$ = Actual temperature, K

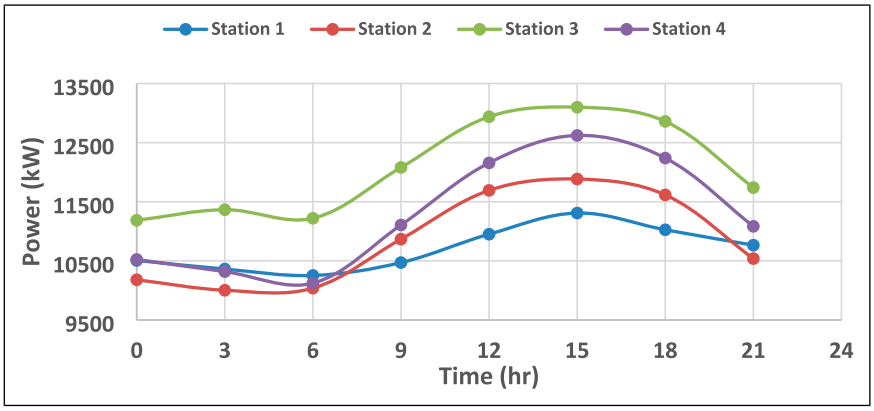



**Figure 16.** Gas compressor power requirement for Scenario 2

**Table 3.** Validation with aspen HYSYS.

| | Gas compressor power (kW) | | |
|---|---|---|---|
| Station number | Analytical | Aspen HYSYS | Absolute deviation (%) |
| 1 | 10463.2 | 10458.2 | 0.048 |
| 2 | 10872.8 | 10872.2 | 0.005 |
| 3 | 12560.0 | 12579.2 | 0.153 |
| 4 | 11714.8 | 11723.8 | 0.077 |
| 5 | 11706.4 | 11715.3 | 0.076 |
| 6 | 11706.4 | 11715.3 | 0.076 |
| 7 | 11313.7 | 11318.1 | 0.039 |
| 8 | 13359.8 | 13388.8 | 0.217 |
| 9 | 12645.4 | 12665.6 | 0.160 |
| 10 | 13721.2 | 13754.8 | 0.245 |
| 11 | 10988.2 | 10989.0 | 0.007 |
| 12 | 10988.2 | 10989.0 | 0.007 |
| 13 | 11642.1 | 11650.2 | 0.070 |
| 14 | 11313.7 | 11318.1 | 0.039 |
| 15 | 11807.4 | 11817.5 | 0.085 |
| 16 | 13071.9 | 13097.3 | 0.194 |
| 17 | 12224.0 | 12239.0 | 0.123 |
| 18 | 7914.5 | 7886.9 | 0.348 |

$P_{ref}$ = Reference pressure, kPa
$P_{act}$ = Actual pressure, kPa

Substituting the corrected mass flow rate with the corrected volume flow rate, noting that the gas compressor under study is a constant-diameter machine. The simplified form of the corrected volume flow rate is obtained by substituting equations (25)–(28) into equation (24):

$$\dot{Q}_c = \dot{Q}_{act}\frac{P_{ref}}{P_{act}}\sqrt{\frac{Z_{act}}{Z_{ref}}}\sqrt{\frac{R_{act}}{R_{ref}}}\sqrt{\frac{k_{ref}}{k_{act}}}\sqrt{\frac{T_{act}}{T_{ref}}} \tag{29}$$

The actual volume flow for the new compressor map was obtained using equation (29) and the scaling factor for the corrected volume flow rate defined by:

$$\dot{Q_{c_SF}} = \frac{\dot{Q_{c_DP}}}{\dot{Q_{c_OEM_DP}}} \tag{30}$$

Where:
$\dot{Q_{c_SF}}$ = Scaling factor for corrected volume flow
$\dot{Q_{c_DP}}$ = Corrected volume flow at the design point, $m^3/h$

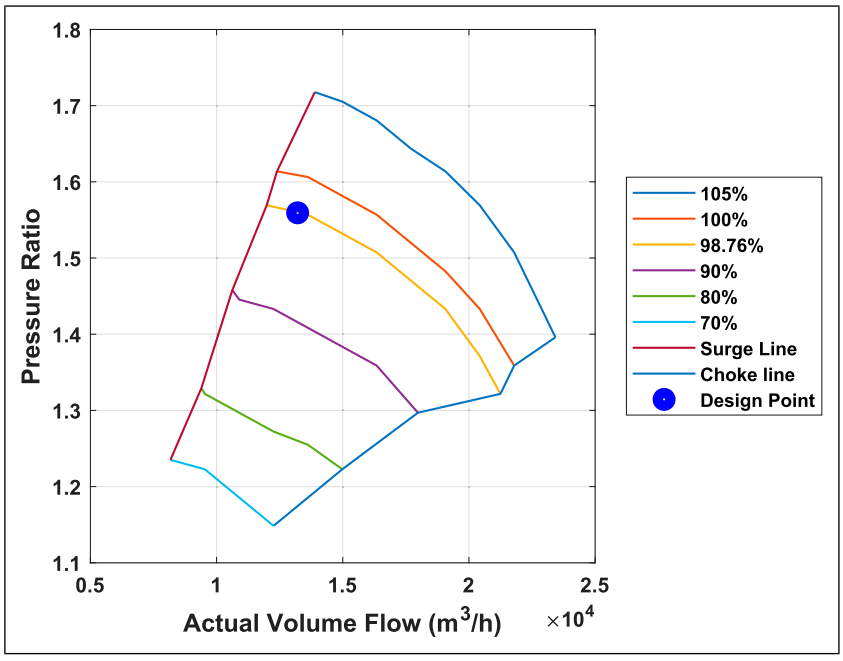



**Figure 17.** Pressure ratio curve for station 3

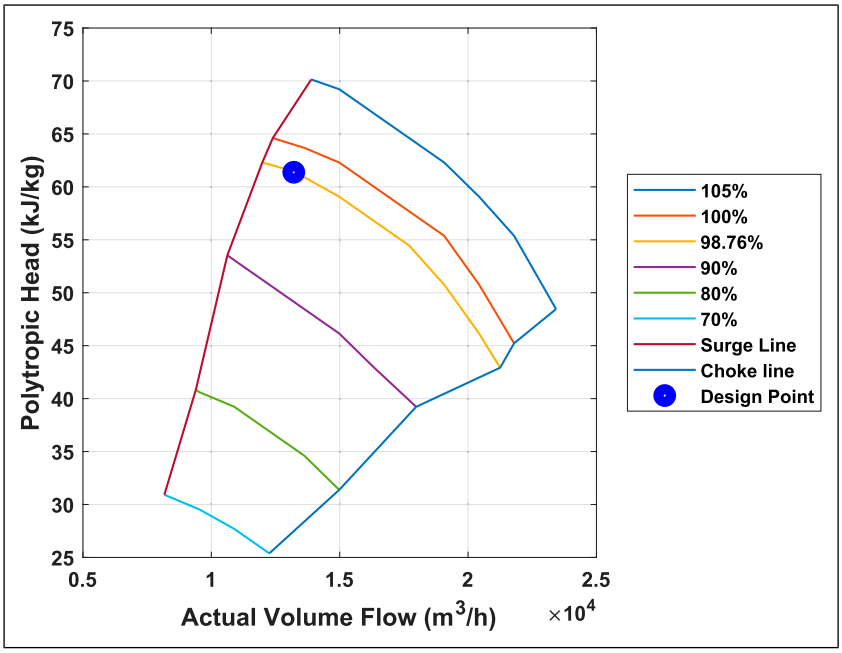



**Figure 18.** Polytropic head curve for station 3

$\dot{Q}_{c_OEM_DP}$ = Corrected volume flow at design point from OEM, $m^3/h$

The following shows the steps utilised in obtaining the pressure ratio curves for the new maps:

i. Obtain the pressure ratio at the design point for the new map
ii. Obtain the pressure ratio at the design point from the original equipment manufacturer's map
iii. Obtain the scaling factor for the pressure ratio at the design point
iv. Generate pressure ratio data at off-design conditions from the original equipment manufacturer map
v. Compute the equivalent pressure ratio at off-design conditions for the new map using the scaling factor obtained from item iii

New gas compressor maps for the pressure ratio were obtained by a scaling factor defined by:

$$PR_{SF} = \frac{PR_{DP} - 1}{PR_{OEM_DP} - 1} \tag{31}$$

Where:
$PR_{SF}$ = Scaling factor for pressure ratio
$PR_{DP}$ = Pressure ratio at design point
$PR_{OEM_DP}$ = Pressure ratio at design point from OEM

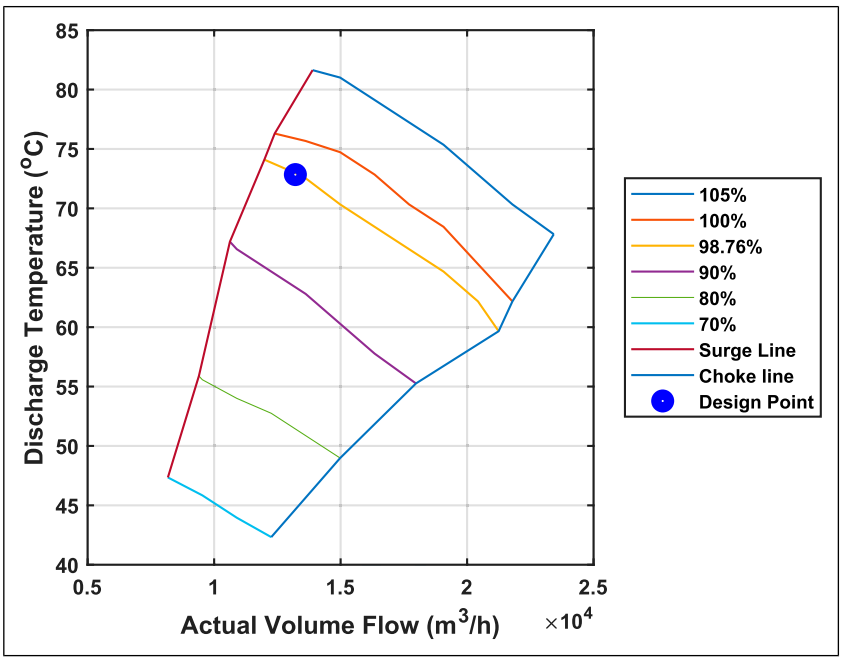



**Figure 19.** Discharge temperature curve for station 3

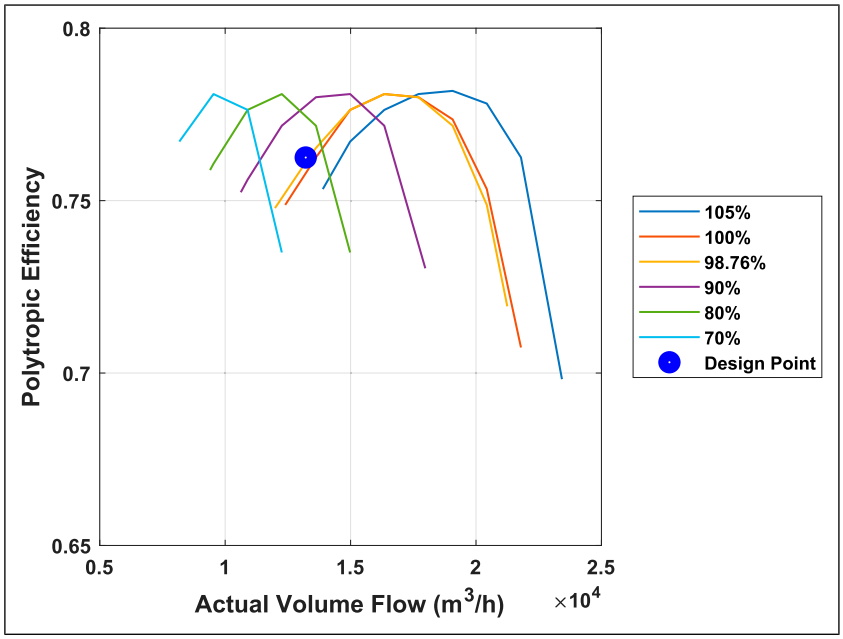



**Figure 20.** Polytropic efficiency curve for station 3

The steps utilised in obtaining the polytropic efficiency, polytropic head and discharge temperature curves for the new maps are as follows:

i. Obtain the polytropic efficiency, polytropic head and discharge temperature at the design point for the new maps
ii. Obtain the polytropic efficiency, polytropic head and discharge temperature at the design point from the original equipment manufacturer maps
iii. Obtain the scaling factors for the polytropic efficiency, polytropic head and discharge temperature at the design point
iv. Generate polytropic efficiency, polytropic head and discharge temperature data at off-design conditions from the original equipment manufacturer maps
v. Compute the equivalent polytropic efficiency, polytropic head and discharge temperature at off-design conditions for the new maps using the scaling factor obtained from item iii

New compressor maps were obtained for the compressor polytropic efficiency, polytropic head and discharge temperature by defining their scaling factors as follows:

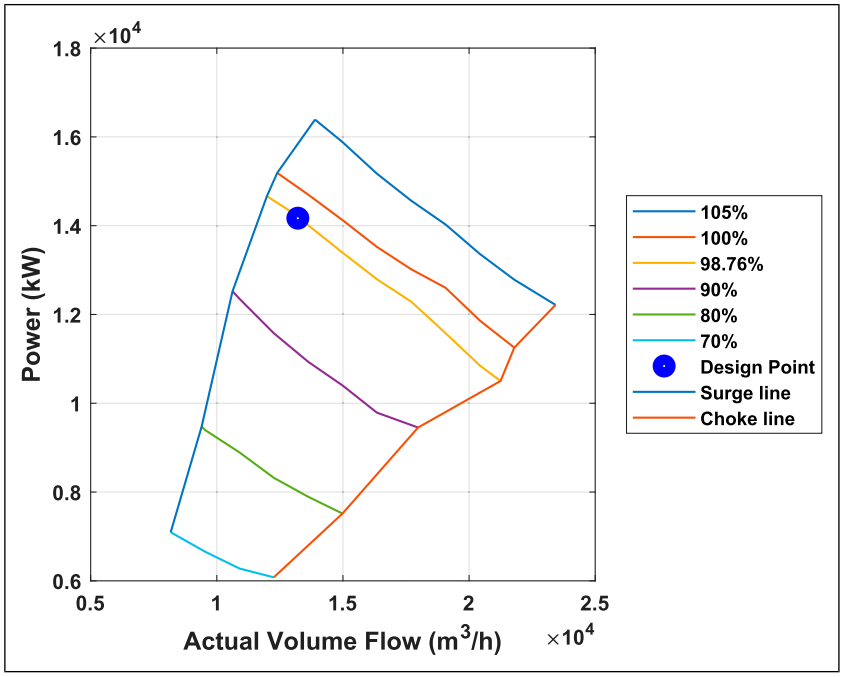



**Figure 21.** Power curve for station 3

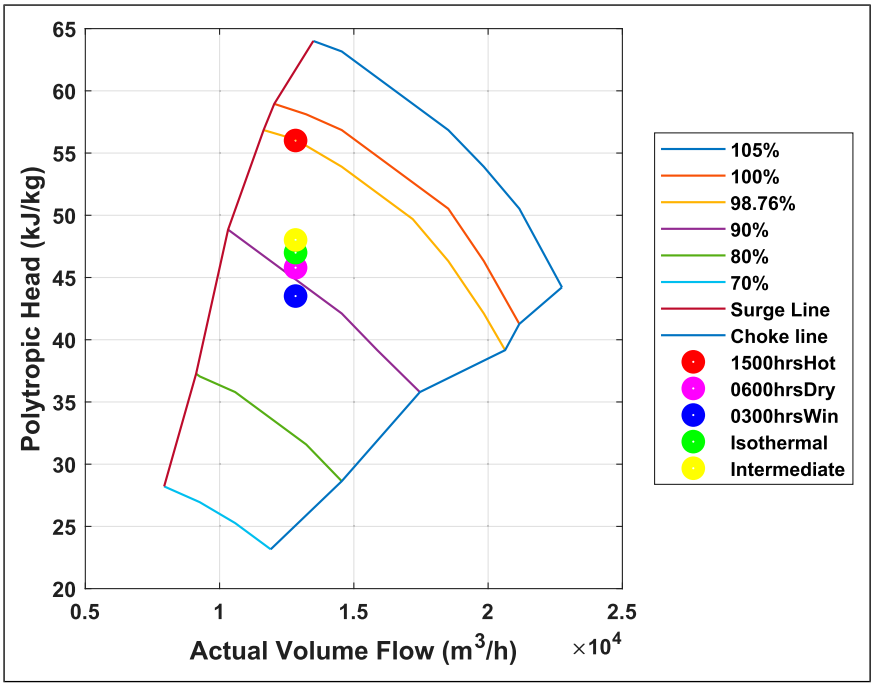



**Figure 22.** Polytropic head curve for station 2 showing operating points in different flow conditions.

$$\eta_{SF} = \frac{\eta_{DP}}{\eta_{OEM_DP}} \quad (32)$$

$$H_{SF} = \frac{H_{DP}}{H_{OEM_DP}} \quad (33)$$

$$T_{SF} = \frac{T_{DP}}{T_{OEM_DP}} \quad (34)$$

$\eta_{DP}$ = Polytropic efficiency at design point
$\eta_{OEM_DP}$ = Polytropic efficiency at design point from OEM
$H_{SF}$ = Scaling factor for polytropic head
$H_{DP}$ = Polytropic head at design point, kJ/kg
$H_{OEM_DP}$ = Polytropic head at design point from OEM, kJ/kg
$T_{SF}$ = Scaling factor for discharge temperature
$T_{DP}$ = Discharge temperature at design point, K

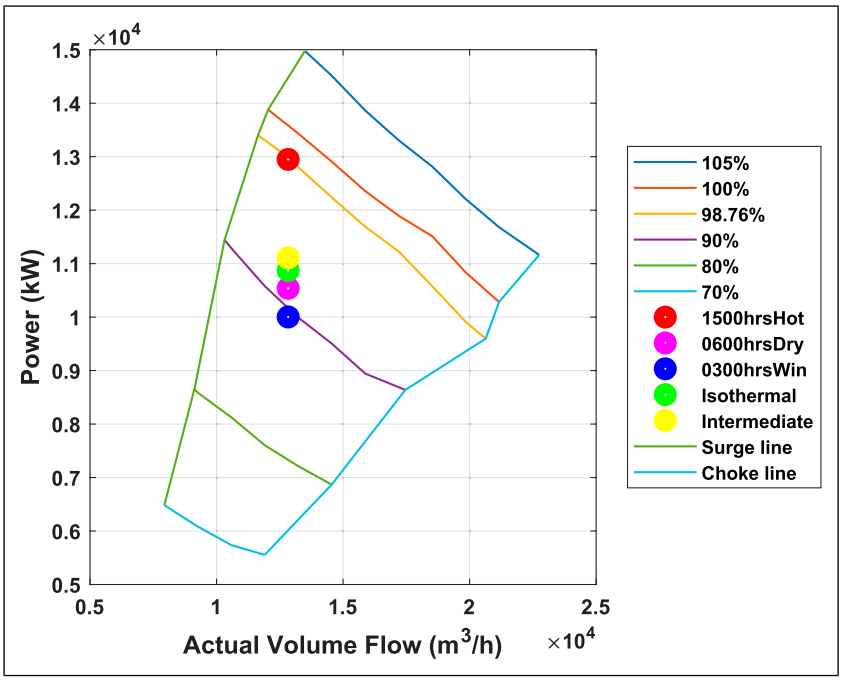



**Figure 23.** Power curve for station 2 showing operating points in different flow conditions.

Where:
$\eta_{SF}$ = Scaling factor for polytropic efficiency
$T_{OEM_DP}$ = Discharge temperature at design point from OEM, K

**Table 4.** Peak, average, and minimum operating-point shifts for station 2

| S/N | Flow conditions | Operating points | |
|---|---|---|---|
| | | Polytropic head (kJ/kg) | Power (kW) |
| 1 | Hot season peak | 56.01 | 12950 |
| 2 | Dry season average | 45.79 | 10539 |
| 3 | Winter season minimum | 43.51 | 10030 |

The following section presents and discusses the results of the TERA framework method utilised in this study.

## Results and discussion

Figure 7 illustrates the pressure gradient of the pipeline at the location of Compressor Station 3.

The pipeline inlet pressure is 9500 kPa. The pressure drops at compressor station 3 vary with pipe distance and gas flow temperature, as described in scenarios 1, 2, and 3. The pressure drop increases with pipe length until it reaches its maximum at 240 km. This is at isothermal and intermediate temperatures of 295.15 K and 305.05 K, depicted by scenarios 1 and 3, respectively. These maximum pressure drops are equivalent to the low pipe-discharge pressures observed at compressor station 3. Considering the non-isothermal condition with a variation in gas flowing temperature, as described by scenario 2. A rise in the gas flow temperature from 295.15 K to 305.05 K at a pipe length of 240 km leads to an increase in the pressure drop. Similarly, a decrease in gas temperature causes lower pressure drops in the pipeline.

The pressure drop variation along the pipeline length at maximum gas-flow temperatures is illustrated in Figure 8 for each compressor station.

The pressure drops to 6785 kPa and 6312 kPa at compressor stations 2 and 3, respectively. Thus, gas compressors are required at these locations to increase the low pressures to the pipeline operating pressures of 9500 kPa. This ensures a continuous supply of natural gas through the pipelines.

### *Effects of gas compressor suction pressure*

Figure 9 displays the gas compressor suction pressure at each compressor station along the pipeline route for scenarios 1 and 3. The suction pressure varies from one station to another.

Compressor stations 10 in scenario 1 and 8 in scenario 3 have the lowest suction pressures. This is because these station locations are associated with the lowest average pipeline pressure. Therefore, high gas compressor power requirements are needed at these locations. Conversely, compressor station 18 has the highest gas-compressor suction pressure in scenarios 1 and 3. This is because this station location is associated with the highest average pipeline pressure. Hence, low gas compressor power are needed at these locations.

Figure 10 shows the gas compressor suction pressures for the winter season at stations 1–4 under non-isothermal gas-flow temperature conditions for scenario 2.

The gas compressor suction pressures are lowest at 15:00 hours, when the ambient temperature is highest. Furthermore, the average pipeline pressure is lowest at this time of day. Therefore, high power is required for the gas compressor. Conversely, the suction pressures are highest at 06:00 hours, when the ambient temperature is lowest. More so, the average pipeline pressure is highest at this time of day. Consequently, low gas-compressor power is required. Furthermore, the results show that for every 1% increase in ambient temperature, the gas compressor suction pressure decreases by an average 0.1%. This finding is valid across the full range of ambient temperatures considered in this study, provided other conditions remain constant.

Therefore, the results indicate that the gas compressor suction pressure depends on pipe distance, elevation, and ambient temperature.

### *Gas compressor pressure ratio at different stations*

The gas compressor pressure ratio, also known as the compression ratio, is defined as the ratio of its discharge pressure to its suction pressure. In this study, the maximum allowable operating pressure (MAOP) of the pipeline is set at 9500 kPa, which corresponds to the discharge pressure of the gas compressor.

Figure 11 displays the compressor pressure ratio at each station along the pipeline route for scenarios 1 and 3.

Compressor station 18 has the lowest pressure ratio for scenarios 1 and 3, as shown in Figure 11. Therefore, this

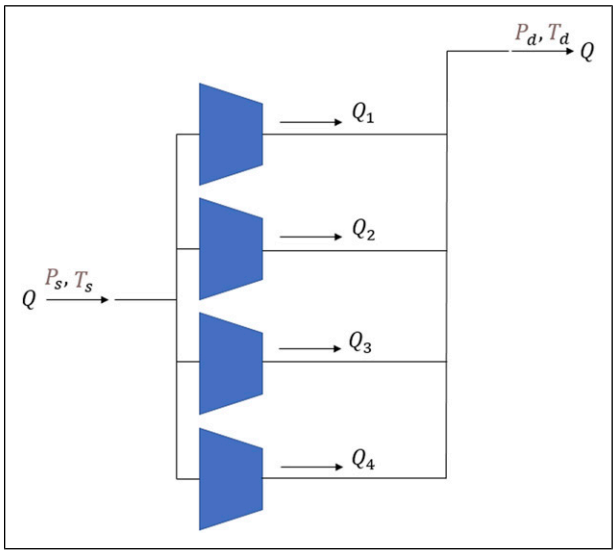



**Figure 24.** Parallel gas compressors arrangement schematic diagram.

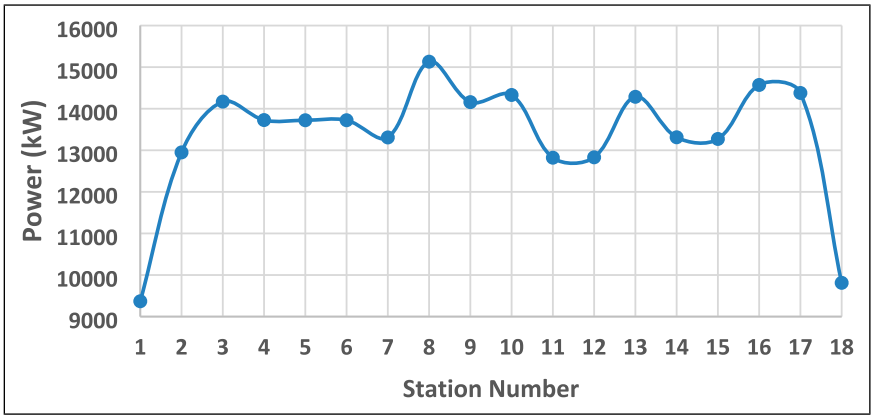



**Figure 25.** Gas compressor power based on maximum ambient temperature in scenarios 1, 2, and 3

station location will require the lowest power from the gas compressor. Conversely, stations 10 and 8 in scenarios 1 and 3, respectively, have the highest gas compressor pressure ratios. Therefore, these station locations will require the highest compressor power.

Figure 12 shows the gas compressor pressure ratios for the winter season at stations 1 to 4, under non-isothermal gas flow temperature conditions for scenario 2. The highest compressor pressure ratios at 15:00 hours will require the highest compressor power. However, the lowest pressure ratios experienced at 06:00 hours will require the lowest compressor power.

### *Gas compressor discharge temperature at different stations*

The discharge temperature is the increase in gas temperature resulting from compression of natural gas. Figure 13 illustrates the gas compressor discharge temperature at each station along the pipeline route for scenarios 1 and 3.

Compressor station 10, which has the highest pressure ratio in Figure 11 for scenario 1, also has the highest discharge temperature. Similarly, Compressor Station 8, which has the highest pressure ratio in Figure 11 for Scenario 3, also has the highest discharge temperature, as shown in Figure 13. Therefore, we conclude that the gas discharge temperature increases with the compression ratio. Thus, a higher gas compression ratio results in a higher discharge temperature of the compressed natural gas. However, compressor station location 10, with the second-highest gas compression ratio in Figure 11 for scenario 3, has the lowest discharge temperature as shown in Figure 13 for scenario 3. This observation is due to the high elevation at this compressor station and the lower suction intermediate temperature at this location compared to other compressor stations.

Figure 14 shows the gas compressor discharge temperature for the winter season at stations 1–4 under non-isothermal gas-flow conditions for scenario 2. The highest gas compressor discharge temperature occurs at 15:00 hours, when the gas compression ratio is at its highest. In contrast, the lowest discharge temperature occurs at 06:00 hours, when the gas compression ratio is at its lowest. Similar explanations can be given for other compressor station locations.

It is beneficial to control the gas compressor discharge temperature within specified limits to optimise gas transport through the pipelines. One way of achieving this is to install a cooling device at the gas compressor discharge point.

### *Gas compressor power at varying flow conditions at different stations*

Figure 15 shows the gas compressor power requirements at each station along the pipeline route for scenarios 1 and 3. Considering scenario 1, compressor station 10 has the highest gas compression power among all stations. This station location is associated with the lowest gas compressor suction pressure, the lowest average pressure, and the highest gas compression ratio. The increase in pipeline distance and elevation results in a corresponding decrease in the gas compressor suction pressure. Therefore, this leads to an increase in the gas compression ratio, the polytropic head, and, thus, the gas compressor power requirement. Moreover, the lower gas compressor power requirement at compressor station 10 in scenario 3, compared to the exact location in scenario 1, is due to the lower suction intermediate temperature at this station. However, the lowest gas compressor power requirement for scenarios 1 and 3 occurs at compressor station 18. This location is associated with the highest gas compressor suction pressure, the highest pipeline average pressure, and the lowest gas compression ratio. Furthermore, gas compressor power decreases with increasing gas compressor suction pressure, due to a lower compression ratio and polytropic head.

Similar explanations could be given for other compressor stations. Consequently, the results indicate that the gas compressor inlet temperature and the characteristics of the compressor station location significantly affect the gas compressor power requirements.

Figure 16 illustrates the gas compressor power requirement for the winter season at stations 1 to 4 under non-isothermal gas-flow temperature conditions for scenario 2. The characteristics of the compressor station location significantly impact the gas compressor's power requirement. These location characteristics depend on the prevailing ambient temperature, the time of day, and the season. More so,

**Table 5.** Criteria for the choice of OEM compressor models.

| Station No | Peak ambient temperature (°C) | Maximum allowable operating pressure (bar) | Decisive compressor power (kW) | OEM maximum discharge pressure (bar) | Required OEM inlet flow (m^3/h) | Gas compressor models |
|---|---|---|---|---|---|---|
| 1 | 15.0 | 95 | 9369 | 155 | 19000 | Siemens STC-SV compressor |
| 2 | 35.4 | 95 | 12950 | 155 | 23000 | Siemens STC-SV compressor |
| 3 | 31.9 | 95 | 14171 | 190 | 23500 | Dresser-Rand DATUM P |
| 4 | 34.7 | 95 | 13727 | 200 | 23500 | Dresser-Rand DATUM C |
| 5 | 34.7 | 95 | 13722 | 200 | 23500 | Dresser-Rand DATUM C |
| 6 | 34.7 | 95 | 13723 | 200 | 23500 | Dresser-Rand DATUM C |
| 7 | 35.6 | 95 | 13309 | 155 | 23500 | Siemens STC-SV compressor |
| 8 | 32.0 | 95 | 15131 | 130 | 24500 | GE centrifugal compressor |
| 9 | 31.9 | 95 | 14158 | 190 | 23500 | Dresser-Rand DATUM P |
| 10 | 25.8 | 95 | 14330 | 130 | 23500 | GE centrifugal compressor |
| 11 | 34.6 | 95 | 12822 | 155 | 23000 | Siemens STC-SV compressor |
| 12 | 34.7 | 95 | 12831 | 155 | 23000 | Siemens STC-SV compressor |
| 13 | 39.6 | 95 | 14287 | 130 | 24000 | GE centrifugal compressor |
| 14 | 35.6 | 95 | 13313 | 155 | 23500 | Siemens STC-SV compressor |
| 15 | 31.9 | 95 | 13273 | 155 | 23000 | Siemens STC-SV compressor |
| 16 | 31.7 | 95 | 14571 | 130 | 24000 | GE centrifugal compressor |
| 17 | 36.2 | 95 | 14379 | 130 | 24000 | GE centrifugal compressor |
| 18 | 40.6 | 95 | 9812 | 155 | 21000 | Siemens STC-SV compressor |

since the pipe diameter, natural gas composition and flow rate are constant. The highest gas compressor power requirement occurs at 15:00 hours, when the ambient temperature is highest across all compressor stations. Conversely, the lowest gas compressor power requirement occurs at 06:00 hours, when the ambient temperature is lowest across all compressor stations. The variation in the gas compressor's power requirement is due to changes in ambient temperature with time of day and station location characteristics. Additionally, the results show a 0.3% average increase in the power required by the gas compressor to

**Table 6.** Parametric sensitivity of compressor power and polytropic head to ±5% variations in key input parameters at station 2 design point.

| Parameter | $\Delta P_{GC}$ (+5%) | $\Delta P_{GC}$ (−5%) | $\Delta H_p$ (+5%) | $\Delta H_p$ (−5%) |
|---|---|---|---|---|
| Inlet temperature, $T_s$ (K) | +1.52% | −1.48% | +1.50% | −1.47% |
| Pressure ratio, *PR* | +0.83% | −0.79% | +0.84% | −0.80% |
| Gas composition (*MW*, kg/kmol) | +0.41% | −0.39% | +0.40% | −0.38% |
| Polytropic efficiency, $\eta_p$ (mechanical) | −1.00% | +1.05% | 0.00% | 0.00% |

Note: $\Delta P_{GC}$ = percentage change in compressor power; $\Delta H_p$ = percentage change in polytropic head. Efficiency ($\eta_p$) does not influence the polytropic head (a thermodynamic quantity independent of efficiency) but does inversely affect power. All results are evaluated at Station 2 design conditions: $T_s$ = 308.56 K, $P_s$ = 6312 kPa, *PR* = 1.505, *MW* = 17.54 kg/kmol, $\eta_p$ = 0.76.

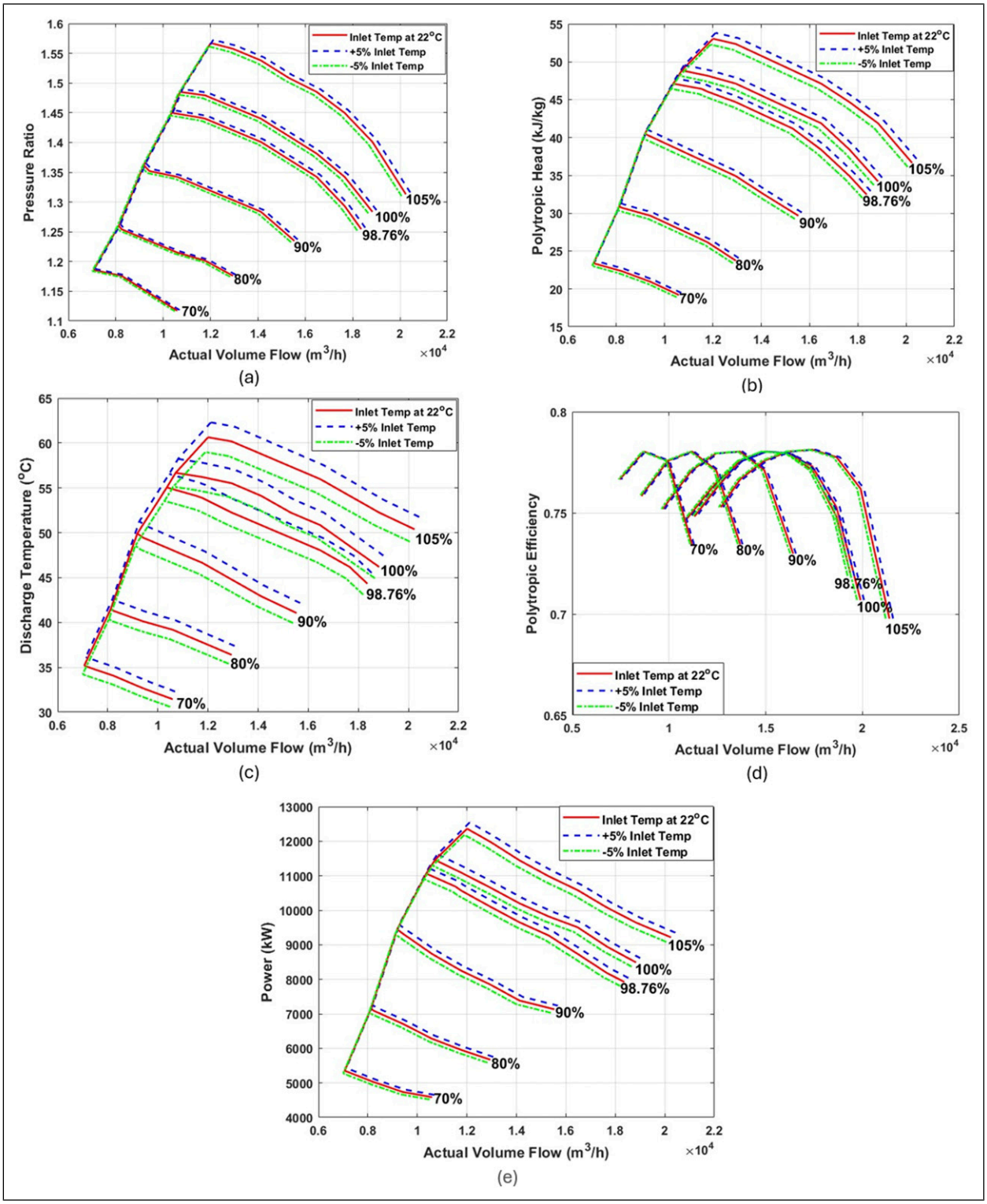



**Figure 26.** Variation of inlet temperature on compressor (a) pressure ratio (b) polytropic head (c) discharge temperature (d) efficiency (e) power.

move the gas for every 1% increase in ambient temperature, across the temperature ranges considered in this study, assuming all other conditions remain the same.

## *Comparison with Aspen HYSYS*

Aspen HYSYS[88] is a process simulation software that can be used in natural gas pipeline applications. The gas compressor power requirements for scenario 1, obtained analytically using a developed MATLAB code, were validated against simulation results from Aspen HYSYS.[27] The Peng-Robinson equation of state is used as the fluid package to determine the natural gas thermodynamic properties. The upstream and downstream material streams were specified and defined in Aspen HYSYS. The centrifugal compressor was connected to the material streams by defining its inlet and outlet streams and specifying its efficiency. Table 3 presents a comparison between the

**Table 7.** Annual operational costs for compressor stations based on Isothermal power requirements.

| Station number | Annual cost (million USD) |
|---|---|
| 1 | 4.67 |
| 2 | 4.85 |
| 3 | 5.60 |
| … | … |
| 10 | 6.12 |
| … | … |
| 18 | 3.53 |
| Total | **~90.66** |

isothermal model results obtained in MATLAB and Aspen HYSYS.

There is strong consistency between the analytical and simulation results from Aspen HYSYS. The maximum absolute percentage difference between the gas compressor powers occurs at compressor station 18, at about 0.348%. Nevertheless, this difference is negligible. Therefore, the analytical methods employed in this study can be applied in the natural gas pipeline industry.

To further characterise the accuracy of the analytical model, the mean absolute percentage deviation (MAPD) across all 18 stations is calculated as 0.035%, confirming that the analytical approach is robust and not merely accurate at isolated points. The relatively larger deviation at Station 18 (0.348%) is attributed to the combined effect of the lowest compression ratio and highest suction pressure at that location, where small absolute differences in thermodynamic property calculations are proportionally amplified. Importantly, 0.348% remains well below the ±1% tolerance commonly accepted in compressor performance analysis for engineering design purposes.

*Measurement and modelling uncertainty analysis.* A structured uncertainty analysis was conducted to assess the combined effect of instrument tolerance and modelling assumptions on the key output performance indicators. The primary sources of uncertainty in the present analytical framework are: (i) ambient temperature measurement, for which meteorological instruments typically carry a tolerance of ±0.5°C; (ii) pipeline inlet pressure specification, with a representative gauge-instrument tolerance of ±0.2%; (iii) compressibility factor $Z$, estimated via the CNGA correlation equation (4) with a reported accuracy of ±1.5% for the pressure and temperature ranges of this study; and (iv) polytropic efficiency $\eta_P$, which carries an OEM map-scaling uncertainty of approximately ±1.0%.

Error propagation through equations (12) and (13) was estimated using a first-order Taylor series expansion. The resulting combined uncertainty in the calculated compressor power $P_{GC}$ is approximately ±2.1% at the 95% confidence level (coverage factor $k = 2$). This bound is consistent with the maximum observed deviation of 0.348% relative to Aspen HYSYS and remains within the ±3% uncertainty typically associated with ISO 5389-compliant compressor performance testing. These findings confirm that the analytical model is suitable for engineering-level design decisions and compressor selection. The ambient temperature measurement uncertainty of ±0.5°C propagates to a power uncertainty of approximately ±0.15%, while the compressibility factor uncertainty dominates at ±1.8%, highlighting that improvements in gas composition measurement or in the fidelity of the thermodynamic equation of state (e.g., using GERG-2008) would yield the most significant reduction in overall model uncertainty.

Having validated the gas compressor power demand against Aspen HYSYS and confirming strong consistency, the next section analyses the gas compressor performance map.

## Gas compressor performance map

The variation of the gas compressor pressure ratio, polytropic head, and discharge temperature with the actual inlet volume flow is illustrated in Figures 17–19, respectively. They show the impact on gas compressor performance.

The results show increases in the gas compressor pressure ratio, polytropic head, discharge temperature, and actual inlet volumetric flow rate with increasing gas compressor shaft rotational speed. However, at a fixed gas compressor shaft rotational speed, the gas volumetric flow rate decreases as the suction pressure decreases, the polytropic head increases, and the gas compressor discharge temperature increases. The increase in the polytropic head is due to a reduction in the gas compressor suction pressure. Moreover, the surge margin increases with rising discharge temperature.

The performance maps above show the gas compressor surge line, the choke line, and the design point.

Figure 20 illustrates the variation in gas compressor polytropic efficiency with actual inlet volume flow at different rotational speeds on the gas compressor performance map for compressor station 3.

The gas compressor polytropic efficiency increases with the actual inlet volume flow rate until it reaches a maximum. Thereafter, it starts to decrease. Additionally, the working point at the design conditions of compressor station 3 has a polytropic efficiency approximately 2% lower than the maximum.

Figure 21 illustrates the variation in gas compressor power requirement at design and off-design conditions, as well as the actual inlet volume flow, at different rotational speeds on the gas compressor performance map for station location 3.

The results show an increase in gas compressor power and actual inlet volumetric flow rate as gas compressor shaft rotational speed increases. However, at a constant gas compressor shaft rotational speed, the gas volumetric flow rate decreases as the gas compressor power requirements increase. This arises from an increase in the polytropic head due to a rise in the gas flow temperature.

## Impacts of operating points at varying flow conditions

Figures 22 and 23 illustrate the polytropic head and the power curves for station 2. They show operating points in different flow conditions.

The results illustrate the effects of varying operating conditions at different points. A change in the location's ambient temperature from 15:00 hours in the hot season to 06:00 hours in the dry season to 03:00 hours in the winter season for the non-isothermal flow conditions of scenario two leads to new operating points. These are illustrated in Figures 22 and 23. However, the gas compressor operating points are fixed at isothermal conditions (scenario 1) and at intermediate flow conditions (scenario 3). At these flow conditions, the temperatures are constant.

Table 4 illustrates the shifts in peak, average, and minimum operating points for station 2.

At 15:00 hours on a hot day, when the highest temperature is recorded, the polytropic head is 56.01 kJ/kg, and the required gas power is 12,950.0 kW. Similarly, at 06:00 hours of the day in the dry season, the polytropic head is 45.79 kJ/kg, and the required gas power is 10,539.0 kW. Furthermore, at 03:00 hours of the day during the winter season, when the temperature is at its lowest, the polytropic head is 43.51 kJ/kg, and the required gas power is 10,030.0 kW. The polytropic head shows a 28.7% operational range that is entirely invisible under the conventional isothermal assumption. Similarly, the peak non-isothermal power at Station 2 is approximately 19.1% above the isothermal estimate, while off-peak power is 7.75% below it. We observed that the gas power required increases with the polytropic head at a constant actual volume flow rate. This occurs due to a rise in the gas temperature. Furthermore, the gas compressor polytropic head increases by an average of 0.3% for each 1% increase in ambient temperature over the temperature range considered in this study. Therefore, the results show that, at constant gas composition and volume flow rate, the natural gas temperature significantly affects gas compressor performance.

Consequently, it is recommended that the working point be kept well away from the compressor stability curve. This study recommends a minimum surge margin of approximately 10% relative to the compressor surge line. This is important for steady operation and to prevent mechanical damage to the compressor. Therefore, the results have demonstrated that all operating points lie within the feasible regions for each scenario considered in this study. The subsequent section illustrates how the gas compressors are selected based on the results of the performance analysis using the TERA framework.

## Gas compressor selection

Gas compressors are chosen based on the performance analysis and economic considerations. This analysis accounts for the highest ambient temperature, gas compression ratio, and power requirements for the gas compressors across all flow conditions considered in the scenarios. This includes decisions on the economic cost of the selected gas compressors. At each compressor station, four identical gas compressors are arranged in parallel. The baseline scenario includes 18 compressor stations along the natural gas pipeline route. Each gas compressor produces the same compression ratio and power and compresses an equivalent volume of natural gas. Figure 24 illustrates a schematic of gas compressors arranged in parallel.

The significant volume flow rate required to be transported through the Trans-Saharan Gas Pipeline route necessitates the selection of parallel gas compressor arrangements. This selection has the advantage of lower gas compressor discharge temperatures than the series arrangement, as it eliminates the need for multiple compression ratios. Therefore, the total gas compressor discharge temperature for this selection will be equivalent to that of a single gas compressor installed at the compressor station with a similar compression ratio.

Figure 25 shows the gas compressor power requirement based on the maximum ambient temperature for all flow conditions described by scenarios 1, 2, and 3 at each compressor station location.

The first gas compressor station is assumed to operate under International Standard Atmosphere conditions. The maximum temperatures were observed at 15:00 hours of the day during the hot season of the year. These guidelines are used to select the appropriate gas compressor models in this study.

Four gas compressor models are chosen based on the gas compressor power requirements at all flow conditions described by scenarios 1, 2, and 3, while considering the economic implications of the selected models. These gas compressor models are inspired by: Siemens' single-shaft pipeline compressor packages STC-SV compressor, General Electric centrifugal compressors, Dresser-Rand DATUM P, and DATUM C compressor trains. The gas compressor models are selected based on their small footprints, engine availability, and project lifecycle costs.

Table 5 summarises the quantitative criteria used to select the OEM-inspired compressor model at each station. The selected compressor models are custom-designed to cover the performance range required for this study. This is in terms of the pipeline's maximum allowable operating pressures, compressor power, and inlet volume flows, with the discharge pressure no less than 95 bar. A 16% power margin is applied to the decisive power to cater for the off-design fluctuations in line with the compressor maps.

Gas turbine models are selected based on the gas compressor power requirements at all flow conditions. However, these are outside the scope of this study. Future studies will incorporate gas turbine performance analysis. The following section utilised a parametric sensitivity analysis to assess the effectiveness of the TERA framework outputs in response to variations in the gas compressor station's key performance indicators.

## Parametric sensitivity analysis

To assess the robustness of the TERA framework outputs to plausible variations in key operational parameters, a one-at-a-time (OAT) parametric sensitivity analysis was performed at the design operating point of compressor station 2, used as the reference case. Each of the four parameters was independently varied by ±5% from its baseline value, whilst all other parameters were held constant. The parameters evaluated were: (i) compressor suction (inlet)

temperature $T_s$, (ii) compression pressure ratio $PR = P_1/P_2$, (iii) gas molecular weight $MW$, as a proxy for gas composition change, and (iv) polytropic efficiency $\eta_p$, as a proxy for variation in mechanical efficiency. The resulting changes in two key station performance indicators — compressor power $P_{GC}$ and polytropic head $H_p$ — are reported in Table 6 as percentage deviations from the baseline.

The results in Table 6 confirm that inlet temperature is the most influential parameter, with a ±5% perturbation producing a ±1.5% change in compressor power and an equivalent ±1.5% change in polytropic head. This finding is consistent with the diurnal power variation observed in the section analysing the gas compressor power at varying flow conditions at different station, where non-isothermal ambient fluctuations directly drive compressor demand. The pressure ratio ranks second in influence (±0.8%), followed by polytropic efficiency (±1.0% on power only) and gas composition through $MW$ (±0.4%). The near-symmetric response across all parameters confirms approximately linear sensitivity within the ±5% perturbation range. These results have two important design implications: first, compressor sizing should account for worst-case inlet temperature, not average conditions; and second, the relatively modest influence of gas composition ($MW$) variation supports the assumption of constant gas composition adopted in this study, as a ±5% change in $MW$ — far larger than normal production variability for this pipeline — produces only a ±0.4% change in power demand. Figure 26 further shows how ±1.5% variation in inlet temperature at station 2 (Figure 26(a)–(c), (e)) and station 3 (Figure 26(d)) influences the compressor pressure ratio, polytropic head, discharge temperature, polytropic efficiency, and power, considering the isothermal temperature conditions of scenario 1 as the baseline. There is a proportional change in the compressor performance indicators with the gas compressor inlet temperature as reported above. Considering Figure 26(c), a ±1.5% variation in inlet temperature leads to a ±2.73% proportional change in the station discharge temperature. Thus, highlighting the need to install a cooling device at the gas compressor discharge point to maintain temperature within specified limits for optimal performance.

Having performed a parametric sensitivity analysis to assess the robustness of the TERA framework, the following section translates the gas compressor power demand into operational costs to fully realise the techno-economic aspect of the TERA framework.

### *Techno-economic and operational impact analysis*

The technical performance analysis presented in the preceding sections has direct and significant implications for the economic and operational viability of the compressor stations. To fully realise the "Techno-economic" aspect of the TERA framework, this section translates the gas compressor power requirements into operational costs, using the business electricity rate for Nigeria of USD 0.051 per kWh.[89,90] However, this business electricity rate does not reflect location-specific pricing but is justified because it serves as a better approximation for financial modelling and scenarios comparison purposes. Particularly, since the project is in its conceptual phase.

The annual operational cost for each compressor station was calculated based on the power requirements from Scenario 1 (Isothermal) (see Table 3) using the formula:

$$\text{Annual Cost (USD)} = \text{Power (kW)} \times \mathbf{24}\,\text{hours/day} \times \mathbf{365}\,\text{days/year} \times \mathbf{0.051}\,\text{USD/kWh}$$

The results, summarised in Table 7, reveal a total annual operating cost of approximately USD 90.66 million for the entire network of 18 stations under isothermal conditions. Station 10, with the highest power requirement of 13,721.0 kW, is also the most expensive to operate, with an annual cost of USD 6.12 million.

However, the critical finding from preceding sections is that power demand is not constant but fluctuates under real-world, non-isothermal conditions (Scenario 2). During the hottest part of the day (15:00 hours), power requirements can be significantly higher. A sensitivity analysis assuming a +10% power increase during daily peaks reveals that operational costs could be underestimated by over USD 56,000 per year for a single station, such as Station 3, totalling millions of dollars across the entire pipeline network. This demonstrates that the isothermal assumption, while simplifying design, risks substantial underestimation of long-term operational expenditures (OPEX).

Furthermore, Nigeria's electricity market is characterised by volatility, with prices influenced by factors such as exchange rates, gas prices, and regulatory changes.[90,91] A sensitivity analysis of a ±10% change in the electricity rate would correspondingly alter the total annual cost by approximately ±USD 9.07 million, highlighting a significant financial risk that must be managed.

These economic insights lead to several strategic operational recommendations:

**Load Management:** Scheduling energy-intensive maintenance during cooler periods (e.g., early morning) could reduce costs.

**Alternative Energy Sources:** The high operational cost strengthens the business case for investing in onsite power generation, such as using pipeline gas for turbine drive or integrating solar power in high-potential regions like Northern Nigeria, to mitigate grid price volatility.

**Financial Hedging:** Securing long-term power purchase agreements (PPAs) could provide price stability and improve the project's financial predictability.

Therefore, this economic analysis confirms that the non-isothermal model is not merely a technical exercise but a crucial tool for accurate financial forecasting, risk assessment, and optimising the total lifecycle cost of the pipeline system.

## Conclusion

This study successfully implemented a Techno-Economic and Environmental Risk Analysis (TERA) framework to

evaluate the performance of gas compressor stations under three distinct thermal-flow scenarios for natural gas pipelines. The comprehensive analysis reveals that:

**Flow thermal regime significantly impacts system performance:**
The assumption of gas temperature behaviour (i.e., isothermal, intermediate, or non-isothermal) fundamentally affects pipeline pressure drops, compressor suction conditions, and power requirements. Non-isothermal analysis most accurately captures real-world operational dynamics, in which an increase in gas flow temperature leads to an increase in pressure drop, and vice versa.

**Station location determines power demand:**
Compressor stations with long pipeline segments and high elevation gain (e.g., Station 10) experience the most challenging operating conditions, characterised by the lowest suction pressures, highest compression ratios, and thus, the highest power requirements.

**Non-isothermal conditions introduce operational variability:**
Under realistic non-isothermal conditions, compressor power exhibits substantial diurnal and seasonal fluctuations, peaking at 15:00 hours during hot seasons and reaching minimums at 06:00 hours during cold seasons. This variability necessitates equipment sizing based on peak demand rather than average conditions.

**Economic implications are substantial:**
The estimated annual operational cost of $90 million under isothermal conditions is subject to significant increases due to non-isothermal fluctuations and regional electricity price volatility, highlighting critical financial planning considerations.

The analytical methodology developed in MATLAB demonstrated excellent agreement with industry-standard Aspen HYSYS simulations, validating its accuracy for compressor performance analysis. The maximum absolute percentage difference in power calculations was merely 0.348% at Station 18 - well within acceptable engineering tolerances. This strong correlation confirms the reliability of the developed models for natural gas pipeline applications. Furthermore, the investigated scenarios comprehensively represent realistic operating conditions encountered in long-distance transmission pipelines, encompassing the full spectrum of temperature variations across geographical routes. Consequently, this study provides pipeline designers with a validated framework for optimising compressor station design and operation in both new projects and existing infrastructure.

## Limitations and future research directions

This study has evaluated the performance of the gas compressor and pipeline system under various gas flow temperature conditions. However, the analysis was performed under the assumption that the gas-flow temperature is equivalent to the location's ambient temperature at the compressor station's suction or discharge point. Future studies could examine the derivation of equations describing the transient flow of gas in pipes. In this approach, the gas temperature will be a function of the pipe length. This would be computed using a numerical model developed to incorporate the energy equation. The analysis would yield a time-dependent temperature profile based on transient, non-isothermal gas flow in the natural gas pipeline. The uncertainty analysis identifies the compressibility factor as the dominant contributor to model uncertainty. Future work will incorporate improvements to the compressibility factor through better gas-composition measurements and higher-fidelity real-gas models, such as GERG-2008.

## Acknowledgements

The authors are grateful to the Petroleum Technology Development Fund of Nigeria (PTDF/ED/PHD/OOB/1386/18), for funding the PhD research that has led to the publication of this paper.

## Declaration of conflicting interests

The authors declared no potential conflicts of interest with respect to the research, authorship, and/or publication of this article.

## Funding

The authors disclosed receipt of the following financial support for the research, authorship, and/or publication of this article: Petroleum Technology Development Fund (PTDF/ED/PHD/OOB/1386/18).

## ORCID iDs

Oluwatayo Babatope Ojo https://orcid.org/0000-0002-1295-9011
Uyioghosa Igie https://orcid.org/0000-0002-2708-0237

## References

1. Ekhtiari A, Dassios I, Liu M, et al. A novel approach to model a gas network. *Appl Sci* 2019; 9(6): 1047. https://doi.org/10.3390/app9061047
2. Abbas AJ, Haruna SK, Burby M, et al. Transitioning to a hydrogen economy: exploring the viability of adapting natural gas pipelines for hydrogen transport through a case study on compression vs. looping. *Gases* 2024; 4(2): 74–96. https://doi.org/10.3390/gases4020005
3. Chen W, Bian R, Xu F, et al. Data-driven flow control for natural gas pipeline networks: optimizing via anomaly detection and residual weight coefficients. *ACS Omega* 2025; 10(34): 39034–39046. https://doi.org/10.1021/acsomega.5c05225
4. Ojo OB, Hegab A and Pilidis P. Impact of compressor station availability on the techno-economics of natural gas pipeline transportation. *Energies* 2025; 18(16): 4243. https://doi.org/10.3390/en18164243
5. Han P, Hua H, Wang H, et al. A universal parallel simulation framework for energy pipeline networks on high-performance computers. *J Supercomputing* 2024; 80(10): 14085–14115. https://doi.org/10.1007/s11227-024-05996-z

6. Wang H, Zhai C, Ma L, et al. Functionality assessment of natural gas distribution networks in post-earthquake scenarios with widespread component failures. *Reliab Eng Syst Saf* 2025; 262: 111134. https://doi.org/10.1016/j.ress.2025.111134
7. Liu ZE, Long W, Chen Z, et al. A novel optimization framework for natural gas transportation pipeline networks based on deep reinforcement learning. *Energy AI* 2024; 18: 100434. https://doi.org/10.1016/j.egyai.2024.100434
8. Ganter S, Martini T, Kopustinskas V, et al. A highly robust gas network simulation approach through an inherently solvable problem formulation for network states far from intended design points. *Appl Math Model* 2024; 127: 297–326. https://doi.org/10.1016/j.apm.2023.12.009
9. Shi G, Yu W, Wang K, et al. Time-dependent economic risk analysis of the natural gas transmission pipeline system. *Process Saf Environ Prot* 2021; 146: 432–440. https://doi.org/10.1016/j.psep.2020.09.006
10. Martini T, Ganter S, Finger J, et al. A robust transient gas network simulation for predicting the dynamics before, during, and after extensive disruptions. *Reliab Eng Syst Saf* 2026; 265: 111465. https://doi.org/10.1016/j.ress.2025.111465
11. Wang C, Wang B, Jia N, et al. An analytical study on the correlations between natural gas pipeline network scheduling decisions and external environmental factors. *Energies* 2025; 18(13): 3274. https://doi.org/10.3390/en18133274
12. Wei J, Zhang J, Xia Y, et al. Research on safety resilience evaluation of gastransmission pipelines in chemical industry parks. *J Loss Prev Process Ind*. 2025; 98: 105739. https://doi.org/10.1016/j.jlp.2025.105739
13. Zhou Y, Fan J, Dai B, et al. A data-driven PCA-hierarchical clustering framework for adaptive risk assessment of gas pipeline networks. *Process Saf Environ Prot* 2025; 202: 107753. https://doi.org/10.1016/j.psep.2025.107753
14. Ojo OB, Igie U and Pilidis P. Techno-economic optimisation of gas compressor station location as a decision variable. In: Proceedings of the ASME Turbo Expo: Power for Land, Sea and Air. London, UK, 24–28 June 2024, Paper no. GT2024 – 126805, pp. 1–13. https://doi.org/10.1115/GT2024-126805
15. Szoplik J. Changes in gas flow in the pipeline depending on the network foundation in the area. *J Nat Gas Sci Eng* 2017; 43(2017): 1–12. https://doi.org/10.1016/j.jngse.2017.03.020
16. Thomas S and Dawe RA. Review of ways to transport natural gas energy from countries which do not need the gas for domestic use. *Energy* 2003; 28(14): 1461–1477. https://doi.org/10.1016/s0360-5442(03)00124-5
17. Hao H, Li J, Ren C, et al. Modeling and optimization of natural gas pipeline networks based on the integration of piecewise linearisation and McCormick relaxation. *Chem Eng Sci*. 2026; 320(C): 122502. https://doi.org/10.1016/j.ces.2025.122502
18. Woldeyohannes A and Majid MAA. Simulation model for natural gas transmission pipeline network system. *Simulat Model Pract Theor* 2011; 19(1): 196–212. https://doi.org/10.1016/j.simpat.2010.06.006
19. Das P, Mohtasim MS, Rowe A, et al. A review of natural gas transportation pipeline optimization and progress towards hydrogen injection: challenges and advances. *Int J Hydrogen Energy* 2025; 124: 102–122. https://doi.org/10.1016/j.ijhydene.2025.03.410
20. Chen J, Zhen Y, Liu Y, et al. Calculation method for failure pressure of oil and gas pipelines with multiple corrosion defects. *Coatings* 2025; 15(7): 774. https://doi.org/10.3390/coatings15070774
21. Zhou D, Jia X, Ma S, et al. Dynamic simulation of natural gas pipeline network based on interpretable machine learning model. *Energy* 2022; 253: 124068. https://doi.org/10.1016/j.energy.2022.124068
22. Fan M, Ao C and Wang X. Comprehensive method of natural gas pipeline efficiency evaluation based on energy and big data analysis. *Energy* 2019; 188: 116069. https://doi.org/10.1016/j.energy.2019.116069
23. Abd AA, Naji SZ and Hashim AS. Effects of non-hydrocarbons impurities on the typical natural gas mixture flows through a pipeline. *J Nat Gas Sci Eng* 2020; 76: 1–6. https://doi.org/10.1016/j.jngse.2020.103218
24. Federal Energy Regulatory Commission. Fact sheet: an interstate natural gas facility on my land? What do I need to know? 2015. https://ferc.gov/interstate-natural-gas-facility-my-land-what-do-i-need-know (accessed 2 June 2024).
25. Liang Y and Hui CW. Convexification for natural gas transmission networks optimization. *Energy* 2018; 158: 1001–1016. https://doi.org/10.1016/j.energy.2018.06.107
26. Pambour KA, Bolado-Lavin R and Dijkema GPJ. An integrated transient model for simulating the operation of natural gas transport systems. *J Nat Gas Sci Eng* 2016; 28: 672–690. https://doi.org/10.1016/j.jngse.2015.11.036
27. Ojo OB. *Introduction of social benefits to the TERA - gas turbines and pipelines*. PhD Thesis. Cranfield University, 2023.
28. Xue W, Wang Y, Liang T, et al. Efficient hydraulic and thermal simulation model of the multi-phase natural gas production system with variable speed compressors. *Appl Therm Eng* 2024; 242: 122411. https://doi.org/10.1016/j.applthermaleng.2024.122411
29. Su H, Zio E, Zhang ZJ, et al. Development of an integrated dynamic model for supply security and resilience analysis of natural gas pipeline network systems. *Pet Sci* 2022; 19(2): 761–773. https://doi.org/10.1016/j.petsci.2021.10.002
30. Rigatos G, Siano P, Sari B, et al. Flatness-based control in successive loops for gas-compressors actuated by IMs and PMSMs. *Int J Robust Nonlin* 2025; 35(14): 6091–6114. https://doi.org/10.1002/rnc.8039
31. Najibi H and Taghavi N. Effect of different parameters on optimum design for high pressure natural gas trunk-lines. *J Nat Gas Sci Eng* 2011; 3: 547–554. https://doi.org/10.1016/j.jngse.2011.06.006
32. Li YG and Suleiman SM. Steady state performance simulation of natural gas pipeline driven by compressor stations. In: ASME Turbo Expo 2016: Turbomachinery Technical Conference and Exposition, Seoul, South Korea, 13–17 June 2016, Paper no. GT2016-56301, pp. 1–11.
33. Hong B, Li X, Di G, et al. An integrated MILP method for gathering pipeline networks considering hydraulic characteristics. *Chem Eng Res Des* 2019; 152: 320–335. https://doi.org/10.1016/j.cherd.2019.08.013
34. Nasir A. *Techno-economic study of gas turbine in pipeline applications*. PhD Thesis. Cranfield University, 2013.
35. Rasmussen P and Kurz R. Centrifugal compressor applications—upstream and midstream. In: *Proceedings of the Thirty-eight Turbomachinery Symposium*. Texas A & M University: Turbomachinery Laboratory, 2009, pp. 169–186.

36. Jung J, Lee WJ, Park S, et al. Improved control strategy for fixed-speed compressors in parallel system. *J Process Control* 2017; 53: 57–69. https://doi.org/10.1016/j.jprocont.2017.02.007
37. Gesser RS, Sartori R, Damo TP, et al. Advanced control applied to a gas compression system of an offshore platform: from modeling to related system infrastructure. *J Pet Sci Eng* 2022; 208: 109428. https://doi.org/10.1016/j.petrol.2021.109428
38. Wilkes J, Pettinato B, Kurz R, et al. Centrifugal compressors. In: Brun K and Kurz R (eds) *Compression Machinery for Oil and Gas. ch. 3*. Gulf Professional Publishing, 2019, pp. 31–133.
39. Jones K, Cortinovis A, Mercangoez M, et al. Distributed model predictive control of centrifugal compressor systems. *International Federation of Automatic Control* 2017; 50(1): 10796–10801. https://doi.org/10.1016/j.ifacol.2017.08.2343
40. Kurz R, Lubomirsky M and Brun K. Gas compressor station economic optimization. *Int J Rotating Mach* 2012; 2012: 1–9. https://doi.org/10.1155/2012/715017
41. Zheng T, Feng H, Wang B, et al. Operational optimization of a cyclic gas pipeline network with consideration of thermal hydraulics. *Ind Eng Chem Res* 2021; 60(6): 2501–2522. https://doi.org/10.1021/acs.iecr.0c04007
42. Giraldo SAC, Supelano R, d'Avila T, et al. Model predictive control with dead-time compensation applied to a gas compression system. *J Pet Sci Eng* 2021; 203: 108580. https://doi.org/10.1016/j.petrol.2021.108580
43. Siemens Energy. Single-shaft centrifugal compressors. 2020. https://www.siemens-energy.com/global/en/home/products-services/product/single-shaft-centrifugal-compressors.html#Performance-data-tab-4 (accessed 21 October 2024).
44. Kurz R and Brun K. Process control for compression systems. *J Eng Gas Turbines Power* 2018; 140(2): 022401. https://doi.org/10.1115/1.4037723
45. Powers KH, Brace CJ, Budd CJ, et al. Modeling axisymmetric centrifugal compressor characteristics from first principles. *J Turbomach* 2020; 142(9): 091010. https://doi.org/10.1115/1.4047616
46. Yu Y, Jiang J, Zhao Y, et al. Numerical research on performance of new structure centrifugal compressor for supercritical CO2 power systems. *Ann Nucl Energy* 2024; 199: 110361. https://doi.org/10.1016/j.anucene.2024.110361
47. Osiadacz AJ and Chaczykowski M. Compressor fuel minimization under transient conditions. In: Pipeline Simulation Interest Group, Atlanta, Georgia, USA, 9–12 May 2017, pp. 1–14.
48. Sriram A, Schlautman J, Varshney M, et al. 3D CFD approach to predict the performance of a centrifugal compressor with surge and choke limits. In: ASME 2021 Gas Turbine India Conference, Virtual, Online, 2–3 December 2021, Paper no. GTINDIA2021-76045, V001T04A008.
49. Li Y, Pei P, Ma Z, et al. Analysis of air compression, progress of compressor and control for optimal energy efficiency in proton exchange membrane fuel cell. *Renew Sustain Energy Rev* 2020; 133: 110304. https://doi.org/10.1016/j.rser.2020.110304
50. Li H, Zuo S and Chen S. Analytical modeling and performance improvement of an electric two-stage centrifugal compressor for fuel cell vehicles. *Proc Inst Mech Eng, Part A: J Power Energy* 2025; 239(1): 19–33. https://doi.org/10.1177/09576509241283612
51. Zhao B, Wu X, Lu Q, et al. An entropy-based assessment of acoustic information confusion at unstable flow occurrence in a centrifugal compressor. *Phys Fluids* 2025; 37(1): 016126. https://doi.org/10.1063/5.0248602
52. Chen S, Zuo S, Wu Z, et al. Comprehensive vibro-acoustic characteristics and mathematical modeling of electric high-speed centrifugal compressor surge for fuel cell vehicles at various compressor speeds. *Mech Syst Signal Process* 2022; 178: 109311. https://doi.org/10.1016/j.ymssp.2022.109311
53. Hassani V and Barzamini R. Design, experimentation, and simulation of dynamic pressure sensor inserts: towards reducing oscillations in measurements. *Mech Syst Signal Process* 2025; 237: 113140. https://doi.org/10.1016/j.ymssp.2025.113140
54. Sun X, Zhang G, He T, et al. Hierarchical evolutionary modeling and performance multi-objective optimization of centrifugal air compressors for fuel cells under multi-operating conditions. *J Clean Prod* 2024; 484: 144355. https://doi.org/10.1016/j.jclepro.2024.144355
55. Yuan W, Lu X, Qiu Y, et al. Exploration of performance optimization strategies for micro-centrifugal compressors in hydrogen fuel cells: a synergistic analysis combining one-dimensional design and three-dimensional flow fields. *Int J Hydrogen Energy* 2025; 131: 229–244. https://doi.org/10.1016/j.ijhydene.2025.04.318
56. Ye W, Zhong S, Shen Y, et al. Predictive control scheme for fuel cell air compressor efficiency enhancement with surge- and choke-constrained awareness. *Adv Theory Simul* 2024; 7(6): 2400284. https://doi.org/10.1002/adts.202400284
57. Cortinovis A, Ferreau H, Lewandowski D, et al. Experimental evaluation of MPC-based anti-surge and process control for electric driven centrifugal gas compressors. *Process Control* 2015; 34: 13–25. https://doi.org/10.1016/j.jprocont.2015.07.001
58. Pronk OI and Bakken LE. Compressor speed impact on positive-slope and second-quadrant performance. In: International Mechanical Engineering Congress and Exposition, Portland, Oregon, 17–21 November 2024, Paper no. IMECE2024-144548, V008T10A054, pp. 1–11.
59. Schulze R and Richter H. Model-based MIN/MAX override control of centrifugal compressor systems. *Franklin Open* 2024; 7: 100084. https://doi.org/10.1016/j.fraope.2024.100084
60. Zagorowska M, Degner M, Ortmann L, et al. Online feedback optimization of compressor stations with model adaptation using gaussian process regression. *J Process Control* 2023; 121: 119–133. https://doi.org/10.1016/j.jprocont.2022.12.001
61. Meira RL, Martins MAF, Kalid RA, et al. Implementable MPC-based surge avoidance nonlinear control strategies for non-ideally modeled natural gas compression systems. *J Nat Gas Sci Eng* 2022; 102: 104573. https://doi.org/10.1016/j.jngse.2022.104573
62. Meira R, Costa G, Kalid R, et al. Improving the centrifugal compressor map through rigorous thermodynamic modeling: an analysis on a natural gas compression station pipeline. *J Nat Gas Sci Eng* 2021; 92: 104006. https://doi.org/10.1016/j.jngse.2021.104006

63. Neto MSSP, Antonio BJN and Yanagihara JI. Impact of hydrogen-enriched methane on the aerodynamic performance of centrifugal compressors: a computational fluid dynamics analysis. *Int J Hydrogen Energy* 2025; 144: 746–759. https://doi.org/10.1016/j.ijhydene.2025.03.189
64. Behrooz HA. Managing demand uncertainty in natural gas transmission networks. *J Nat Gas Sci Eng* 2016; 34: 100–111.
65. Misté GA and Benini E. Turbojet engine performance tuning with a new map adaptation concept. *J Eng Gas Turbines Power* 2014; 136(7): 1–8.
66. Hosseinimaab SM and Tousi AM. A new approach to off-design performance analysis of gas turbine engines and its application. *Energy Convers Manag* 2021; 243: 114411. https://doi.org/10.1016/j.enconman.2021.114411
67. Deng W, Ren G, Jia L, et al. Multi-dimensional simulations for extensive off-design conditions of gas turbines by iterative-coupled methods using different characteristic maps of coaxial compressor and turbine. *Case Stud Therm Eng* 2025; 72: 106290. https://doi.org/10.1016/j.csite.2025.106290
68. Huang Q, Gu X, Zhang H, et al. An adaptive performance map generation method through shape feature fusion for the gas turbine compressor. *Energy* 2025; 320: 135405. https://doi.org/10.1016/j.energy.2025.135405
69. Wang Y, Wang Z, Wang X, et al. A novel performance adaptation method for aero-engine matching over a wide operating range. *J Glob Power Propuls Soc* 2024; 8: 154–165. https://doi.org/10.33737/jgpps/186055
70. Wang B and Xuan Y. Heuristic deepening of aero engine performance analysis model based on thermodynamic principle of variable mass system. *Energy* 2024; 306: 132481. https://doi.org/10.1016/j.energy.2024.132481
71. Albusaidi W and Pilidis P. An iterative method to derive the equivalent centrifugal compressor performance at various operating conditions: part I: modelling of suction parameters impact. *Energies* 2015; 8(8): 8497–8515. https://doi.org/10.3390/en8088497
72. Thomyapitak T, Saengsikhiao P, Vessakosol P, et al. A study on the energy efficiency of an energy management system for convenience stores. *Energies* 2024; 17(19): 4941. https://doi.org/10.3390/en17194941
73. Osiadacz AJ and Chaczykowski M. Comparison of isothermal and non-isothermal pipeline gas flow models. *Chem Eng J* 2001; 81(1-3): 41–51. https://doi.org/10.1016/s1385-8947(00)00194-7
74. Farzaneh-Gord M and Rahbari HR. Unsteady natural gas flow within pipeline network, an analytical approach. *J Nat Gas Sci Eng* 2016; 28: 397–409. https://doi.org/10.1016/j.jngse.2015.12.017
75. Sanaye S and Mahmoudimehr J. Technical assessment of isothermal and non-isothermal modelings of natural gas pipeline operational conditions. *Oil Gas Sci Technol* 2012; 67(3): 435–449. https://doi.org/10.2516/ogst/2011117
76. Farzaneh-Gord M, Rahbari HR, Bajelan M, et al. Investigation of hydrate formation in natural gas flow through underground transmission pipeline. *J Nat Gas Sci Eng* 2013; 15: 27–37. https://doi.org/10.1016/j.jngse.2013.09.001
77. López-Benito A, Tenreiro FJE and Gutiérrez-Pérez LC. Steady-state non-isothermal flow model for natural gas transmission in pipes. *Appl Math Model* 2016; 40(23-24): 10020–10037. https://doi.org/10.1016/j.apm.2016.06.057
78. Yang S and Xuejiang C. Real-time simulation and abnormal condition recognition of series compressor system based on digital twin. *Digital Eng* 2025; 7: 100059.
79. Kai W, Hailong X, Ming X, et al. Digital twin-driven intelligent control of natural gas flowmeter calibration station. *Measurement* 2023; 217: 113140.
80. Tinggong K, Ruixin B, Jianmin R, et al. Performance change prediction of stoner pipeline simulator simulation centrifugal compressor based on Whale Optimization Algorithm-enhanced back-propagation neural network. *Proc Inst Mech Eng E J Process Mech Eng* 2025; 0(0): 1–16.
81. Zexi W, Xu Z, Chen L, et al. Research on performance prediction of modeling designed centrifugal compressor based on similarity and scaling laws informed neural networks. *Proc IMechE Part D: J Automobile Engineering* 2025; 0(0): 1–16.
82. Tukur N. *Techno-economics of natural gas pipeline compression system*. PhD Thesis. Cranfield University, 2018.
83. Menon ES. *Gas pipeline hydraulics*. Taylor & Francis, 2005.
84. Menon ES. *Transmission pipeline calculations and simulations manual*. Elsevier Inc, 2015.
85. Liu E, Guo B, Lv L, et al. Numerical simulation and simplified calculation method for heat exchange performance of dry air cooler in natural gas pipeline compressor station. *Energy Sci Eng* 2020; 8(6): 2256–2270. https://doi.org/10.1002/ese3.661
86. Demissie A, Zhu W and Belachew C. A multi-objective optimization model for gas pipeline operations. *Comput Chem Eng* 2017; 100: 94–103. https://doi.org/10.1016/j.compchemeng.2017.02.017
87. Berdanier RA, Smith NR, Fabian JC, et al. Humidity effects on experimental compressor performance-corrected conditions for real gases. *J Turbomach* 2015; 137(3): 1–10. https://doi.org/10.1115/1.4028356
88. Aspen Technology Incorporation. *Gas compression analysis*, 2023. https://www.aspentech.com/en/applications/engineering/gas-compression-analysis (accessed 7 January 2026).
89. *Nigerian electricity regulatory commission*. Tariff & market. 2024. https://nerc.gov.ng/index.php/home/tariff/ (accessed 25 August 2025).
90. GlobalPetrolPrices. Electricity prices in Nigeria. 2024. https://www.globalpetrolprices.com/Nigeria/electricity_prices/ (accessed 25 August 2025).
91. Okoduwa O. *NERC raises electricity price for band A customers to N225*. BusinessDay Nigeria, 2024. https://businessday.ng/news/article/nerc-raises-electricity-price-for-band-a-customersto-n225/ (accessed 25 August 2025).


# Appendix

## Nomenclature

| | |
|---|---|
| $a_{act}$ | Actual sound speed (m/s) |
| $a_{ref}$ | Sound speed at reference condition (m/s) |
| $D$ | Pipe diameter (mm) |
| $E$ | Pipeline efficiency factor |
| $G$ | Gas gravity |

$H_1$ Upstream elevation (m)
$H_2$ Downstream elevation (m)
$H_{DP}$ Polytropic head at design point (kJ/kg)
$H_{OEM_DP}$ Polytropic head at design point from OEM (kJ/kg)
$H_p$ Polytropic head (kJ/kg)
$H_{SF}$ Scaling factor for polytropic head
$k$ Isentropic exponent
$k_{act}$ Actual polytropic exponent
$k_{ref}$ Polytropic exponent at reference condition
$L$ Pipe length (km)
$L_e$ Pipe equivalent length (km)
$MW$ Gas molecular weight, (kg/kmol)
$m$ Mass flow rate (kg/s)
$m_{act}$ Actual mass flow rate (kg/hour)
$\dot{m}_c$ Corrected mass flow rate (kg/hour)
$n$ Polytropic exponent
$\eta_{DP}$ Polytropic efficiency at design point
$\eta_{OEM_DP}$ Polytropic efficiency at design point from OEM
$\eta_p$ Polytropic efficiency
$\eta_{SF}$ Scaling factor for polytropic efficiency
$P$ Total pressure (kPa)
$P_{act}$ Actual pressure (kPa)
$P_{ref}$ Reference pressure (kPa)
$P_{avg}$ Average pressure (kPa)
$P_b$ Base pressure (kPa)
$P_1$, $P_d$ Discharge pressure, Pipe inlet pressure (kPa)
$P_2$, $P_s$ Suction pressure, Pipe outlet pressure (kPa)
$P_{GC}$ Gas compressor power (kW)
$\Delta P$ Pressure drop (kPa).

## Subscripts

*air* Air
1 Discharge, isothermal, inlet, Upstream
2 Suction, non-isothermal, outlet, Downstream
3 Intermediate
*act* Actual
*avg* Average
*b* Base
*c* Corrected
d Discharge
*DP* Design point
*e* Equivalent
*f* Flow
$PR_{SF}$ Scaling factor for pressure ratio
$PR_{DP}$ Pressure ratio at design point
$PR_{OEM_DP}$ Pressure ratio at design point from OEM
$\rho_s$ Suction density (kg/m$^3$)
$\rho_{act}$ Actual gas density (kg/m$^3$)
$\rho_{ref}$ Reference gas density (kg/m$^3$)
Q Gas flow rate (m$^3$/day)
$Q_{act}$ Actual volume flow rate (m$^3$/hour)
$R$ Gas constant (kJ kg$^{-1}$ K$^{-1}$)
$\dot{Q}_c$ Corrected volume flow rate (m$^3$/hour)
$\dot{Q}_{c_SF}$ Scaling factor for corrected volume flow
$\dot{Q}_{c_DP}$ Corrected volume flow at the design point (m$^3$/hour)
$\dot{Q}_{c_OEM_DP}$ Corrected volume flow at design point from OEM (m$^3$/hour)
$R_{act}$ Actual gas constant (kJ kg$^{-1}$ K$^{-1}$)
$R_{ref}$ Gas constant at reference condition (kJ kg$^{-1}$ K$^{-1}$)
$s$ Elevation adjustment parameter
$T_{act}$ Actual temperature (K)
$T_b$ Base temperature (K)
$T_{DP}$ Discharge temperature at design point (K)
$T_f$ Gas flow temperature (K)
$T_{OEM_DP}$ Discharge temperature at design point from OEM (K)
$T_{ref}$ Reference temperature (K)
$T_{SF}$ Scaling factor for discharge temperature
$T_1$, $T_d$ Gas compressor discharge temperature (K)
$T_2$, $T_s$ Gas compressor suction temperature (K)
$v$ Specific molar volume (m$^3$/kmol)
$y$ Volume fraction
$Z$ Compressibility factor
$Z_{act}$ Actual compressibility factor
$Z_{avg}$ Average gas compressibility factor
$Z_1$ Compressibility factor at discharge condition
$Z_2$ Compressibility factor at suction condition
$Z_{ref}$ Compressibility factor at reference condition
*GC* Gas compressor
*GC*1 Gas compressor, isothermal condition
*GC*2 Gas compressor, non-isothermal condition
*GC*3 Gas compressor, intermediate condition
*j* Component of gas mixture
*OEM* Original equipment manufacturer
*p* Polytropic
*ref* Reference
*s* Suction
*SF* Scaling factor.



https://dspace.org/

# A novel application of TERA framework for gas compressor station performance analysis using thermal modelling assumptions

**Ojo, Oluwatayo Babatope; Hegab, Abdelrahman; Igie, Uyioghosa; Pilidis, Pericles**

**2026-12-31**
Sage
https://doi.org/10.1177/09576509261456450
Ojo OB, Hegab A, Igie U, Pilidis P. (2026) A novel application of TERA framework for gas compressor station performance analysis using thermal modelling assumptions. Proceedings of the Institution of Mechanical Engineers, Part A: Journal of Power and Energy, Available online 1 June 2026

Downloaded from a DSpace repository. https://dspace.org/